iScience

CellPress

Article

Electrical Polarization Enables Integrative Quality Control during Bacterial Differentiation into Spores

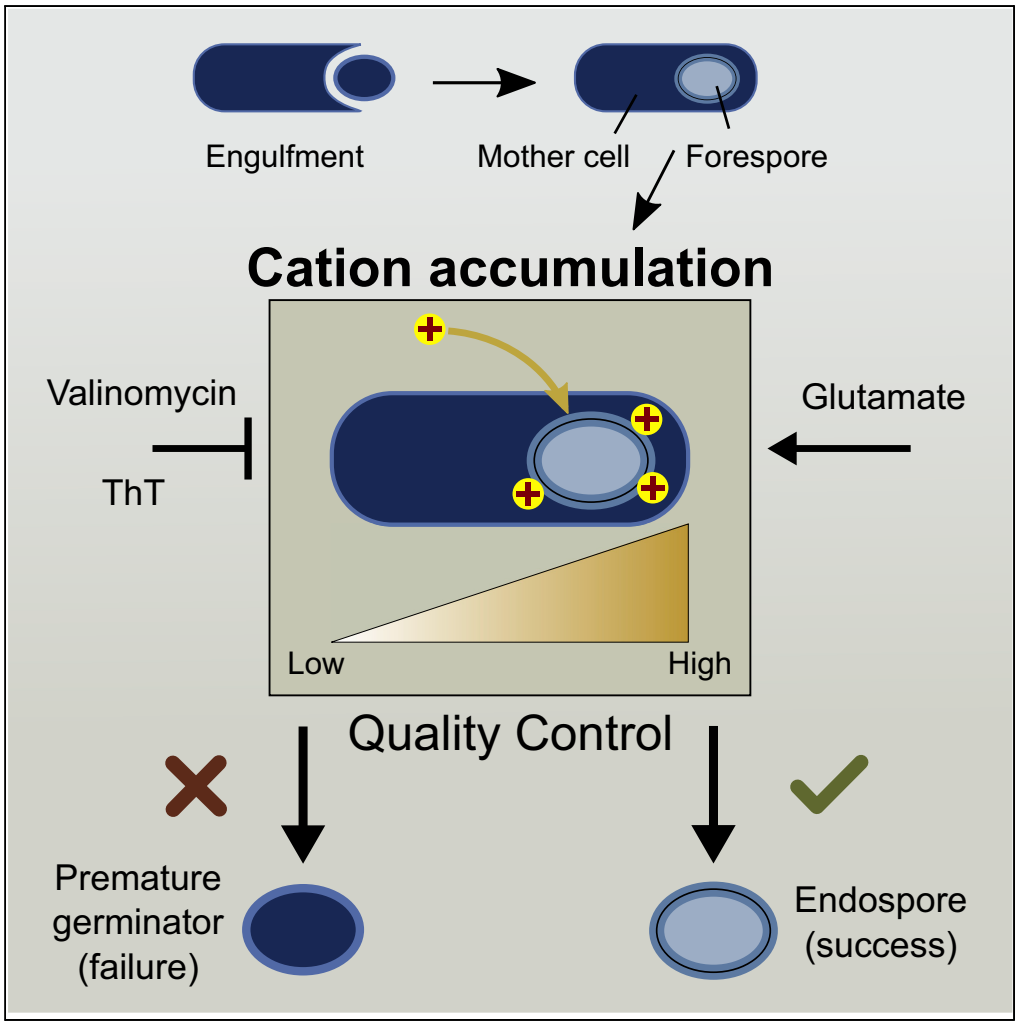

Teja Sirec, Jonatan M. Benarroch, Pauline Buffard, Jordi Garcia-Ojalvo, Munehiro Asally

m.asally@warwick.ac.uk

HIGHLIGHTS

Quality control during bacterial sporulation is coupled with cation accumulation

Cation accumulation prevents premature germination

Cation accumulation integrates information on morphological defects and environments

Spores are less fit when sporulated with Thioflavin T

Sirec et al., iScience *16*, 378–389
June 28, 2019
https://doi.org/10.1016/j.isci.2019.05.044

iScience

CellPress

Article

Electrical Polarization Enables Integrative Quality Control during Bacterial Differentiation into Spores

Teja Sirec,[1] Jonatan M. Benarroch,[1,2] Pauline Buffard,[1] Jordi Garcia-Ojalvo,[5] and Munehiro Asally[1,3,4,6,*]

SUMMARY

Quality control of offspring is important for the survival of cells. However, the mechanisms by which quality of offspring cells may be checked while running genetic programs of cellular differentiation remain unclear. Here we investigated quality control during sporulating in *Bacillus subtilis* by combining single-cell time-lapse microscopy, molecular biology, and mathematical modeling. Our results revealed that the quality control via premature germination is coupled with the electrical polarization of outer membranes of developing forespores. The forespores that accumulate fewer cations on their surface are more likely to be aborted. This charge accumulation enables the projection of multi-dimensional information about the external environment and morphological development of the forespore into one-dimensional information of cation accumulation. We thus present a paradigm of cellular regulation by bacterial electrical signaling. Moreover, based on the insight we gain, we propose an electrophysiology-based approach of reducing the yield and quality of *Bacillus* endospores.

INTRODUCTION

The significances of ion dynamics in bacterial signaling have been uncovered in the last few years (Lee et al., 2017). Cells within *Bacillus subtilis* biofilms can communicate with each other through electrical signaling mediated by the gating of K^+ channels (Prindle et al., 2015). This bacterial electrical signaling increases the fitness of the population by enabling metabolic co-dependence within a biofilm (Liu et al., 2015) and nutrient time sharing of distant biofilms (Liu et al., 2017). A recent study also revealed that the bacterial electrical signaling can attract motile cells in a species-independent manner (Humphries et al., 2017). In *E. coli*, rapid change in membrane potential mediated by the opening of Ca^{2+} channels is crucial for the response to mechanical stresses (Bruni et al., 2017). As a result of these pioneering studies, bacterial electrical signaling concerning the ion dynamics has become an exciting avenue of research, which is, however, still largely uncharted. A particularly important unanswered question is how electrical dynamics interplays with complex genetic signaling processes (e.g., cellular differentiation). How genetically regulated processes interplay with environmental factors and physiological states is a timely and important research topic broadly in biology (Prindle et al., 2012; Taheri-Araghi et al., 2015; Willis et al., 2016). This is because, although molecular biological interactions are well studied in controlled experimental condition, still little is known about the interplay between genetic programs and physiological states. Having this in mind, we investigated the *B. subtilis* spore formation with a focus on the dynamics of cations and quality control.

Sporulation of *B. subtilis* is among the best-characterized bacterial cellular differentiation processes (Lopez-Garrido et al., 2018; Narula et al., 2016). Over five decades of in-depth genetic studies and high-throughput analyses have identified the genes and proteins governing this differentiation process (Eijlander et al., 2014; Mao et al., 2011). The principles of the cellular decision making, leading to the commitment to sporulation, have been deciphered by single-cell time-lapse microscopy and mathematical modeling (Kuchina et al., 2011; Narula et al., 2015). These extensive bodies of research have resulted in a good understanding of the genetic regulatory system driving sporulation. Briefly, the differentiation into endospores begins with phosphorylation of the master transcription factor Spo0A, which leads to the "commitment" defined by the irreversible formation of an asymmetric septum. The septum formation triggers the multistage differentiation program regulated by compartment-specific sporulation sigma factors, resulting in the genetically regulated developmental processes: forespore engulfment, cortex synthesis, coat assembly, and mother-cell lysis. Owing to the mode of formation, the outer spore membrane has opposite polarity with respect to the inner spore membrane (Wilkinson et al., 1975) (Figure 1A).

[1]School of Life Sciences, The University of Warwick, Coventry CV4 7AL, UK

[2]Warwick Medical School, The University of Warwick, Coventry CV4 7AL, UK

[3]Warwick Integrative Synthetic Biology Centre, The University of Warwick, Coventry CV4 7AL, UK

[4]Bio-electrical Engineering Innovation Hub, The University of Warwick, Coventry CV4 7AL, UK

[5]Department of Experimental and Health Sciences, Universitat Pompeu Fabra, 08003 Barcelona, Spain

[6]Lead Contact

*Correspondence: m.asally@warwick.ac.uk

https://doi.org/10.1016/j.isci.2019.05.044

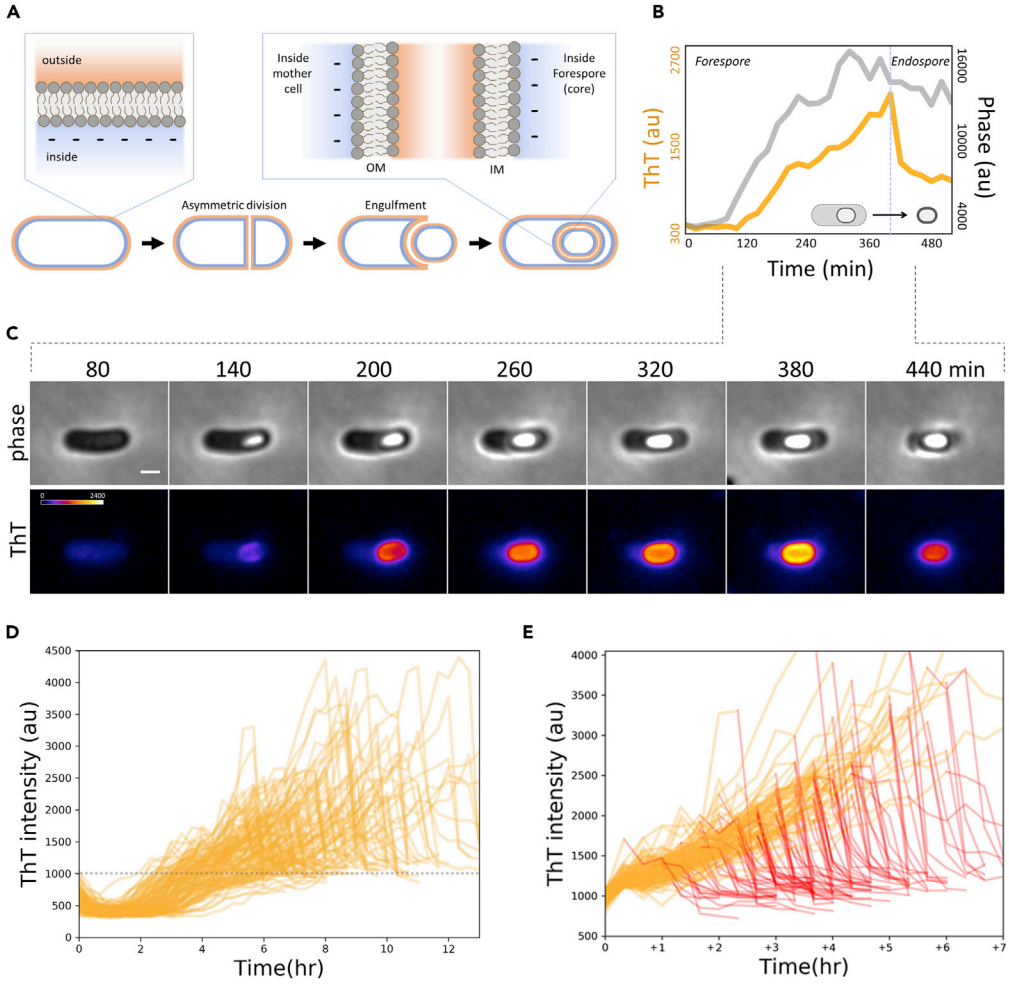

Figure 1. Single-cell Dynamics of a Cationic Dye Revealed a Gradual Increase on Forespores and Sudden Drop upon Mother-Cell Lysis

(A) Illustrative diagram showing the membrane polarities of a sporulating cell. Engulfment process results in forespore membranes with opposite polarities to each other. Quality control works during late sporulation (stage IV-VI) where protective layers are assembled and matured.

(B) Time series of the mean intensities of phase contrast (gray) and ThT (orange) in spore region. The data correspond to the panel (C). ROIs (region of interest) used for the measurements are shown in Figure S1. ThT was added at 10 μM.

(C) Film-strip images showing the phase-contrast (upper) and ThT (lower) of a live single-cell sporulating cell. Scale bar, 1 μm. Color scale for ThT intensity is shown in the left-end panel for ThT. Film-strip is a representative of successfully sporulating cells from twenty-nine independent experiments.

(D) Time series of single-cell ThT fluorescence dynamics from 122 forespores. Forespore regions of ThT intensity were measured until 1 h after mother-cell lysis. All time series qualitatively follow the pattern represented in panel (C) but a great degree of heterogeneity between cells. The dashed line represents the value used for alignment in panel (E).

(E) The dataset shown in panel (D) was aligned to the frame it first reaches ThT intensity value 1,000. Time series after reaching maximum are highlighted in red. ThT increases at a relatively finite rate. A great degree of heterogeneity in timing of mother-cell lysis was observed (red lines). Histograms of the late-sporulation duration with and without ThT are shown in Figures S3 and S4.

Although it is well established that sporulation is regulated by a complex genetic program, it is also evident that the process is subject to a variety of internal and external conditions. Poorly developing spores are eliminated from the population through the quality control mediated by Clp proteases and GerA-dependent premature germination (Ramírez-Guadiana et al., 2017b; Tan et al., 2015). Intriguingly, the quality (e.g., resistance and germination properties) of endospores differs depending on the environmental conditions during sporulation (Nguyen Thi Minh et al., 2011; Rose et al., 2007). For example, endospores

produced at high temperature (~50°C) exhibit higher resistance against heat (~100°C) (Palop et al., 1999). A recent study also suggested that the timing of sporulation affects the spore quality (Mutlu et al., 2018). It is worth noting that such condition-dependent variability of spores is recognized as a major challenge in food industries since it precludes the reliable standardization of the sterilization procedures (Eijlander et al., 2011). However, despite these observations demonstrating the phenotypic plasticity of endospores, the mechanism by which diverse environmental factors and morphological properties affect the sporulation process remains unknown.

We hypothesized that diverse morphological properties and environmental factors can be sensed through electrophysiological dynamics of cells during sporulation, which provides an orthogonal dimension to the complex genetic program of spore differentiation. We characterized the dynamics of cationic molecules during late sporulation (stage IV-VI) of *B. subtilis*. Our single-cell time-lapse microscopy measurements, combined with examinations of genetic mutant strains and minimalistic computational simulations, suggest that the success rate of endospore formation depends on the cation accumulation to the forespore surfaces. Specifically, spore formation is more likely to be completed when forespores accumulate high levels of cations on their surface. Intriguingly, this sensing mechanism enables the quality control to be responsive not only to forespore morphogenetic errors but also to the external environments. Thus, the electrostatic attraction during late sporulation provides a molecular-level insight to the mechanism that enables integrative quality control for spore formation. Finally, in the light of the findings we gained, we succeed in promoting the failure of sporulation using Thioflavin T (ThT) while at the same time decreasing the resistance property of endospores against wet heat.

RESULTS

Single-Cell Measurements of Cation Accumulation Dynamics during Sporulation

To investigate the electrostatic dynamics during late sporulation, we performed time-lapse fluorescence microscopy with sporulating *B. subtilis* cells. ThT is a membrane-permeable cationic dye that has been used with *B. subtilis* (Humphries et al., 2017; Lee et al., 2019; Liu et al., 2017; Prindle et al., 2015; Stratford et al., 2019). Hence, we decided to utilize it as an indicator for electrical polarity during forespore development. Single-cell measurements of ThT fluorescence revealed a gradual increase of the signal on a developing forespore, which then rapidly drops upon mother-cell lysis (Figures 1B and 1C, and Video S1). The fluorescence signal was seen intensely on the peripheral regions of the forespores (Figures 1C and S2). The temporal increase in ThT fluorescence was preceded by the increase in phase-contrast channel, which coincides with the pH drop in the core compartment (Figure S3 and Video S2). The rapid drop of the ThT signal upon mother-cell lysis indicates that ThT associates with the forespore surface in a dynamic manner. The experiments with another positively charged lipophilic dye, TMRM (Kralj et al., 2011; Lo et al., 2007), exhibited the same dynamics as ThT (Figure S4, and Video S3, see also Supplemental Information). These results indicate that the forespore surfaces polarize negatively during late sporulation. We note that the forespore surface is defined here as in the electrochemical sense: the membrane can act as an insulator, whereas spore coat and crust layers do not act as diffusion barriers for small ions owing to their porous structures with the exclusion size of 2–8 kDa (Driks, 1999; Plomp et al., 2014).

We next performed single-cell tracking of ThT dynamics with the cells that produced phase-bright endospores (n = 122). For individual cells, ThT intensity on the forespore compartment was measured until 1 h after the mother-cell lysis. All time series follow the pattern presented in Figures 1B and 1C; explicitly, ThT intensity increases gradually and drops rapidly upon mother-cell lysis. However, there is a large degree of heterogeneity between individual cells (Figure 1D). To better understand the observed heterogeneity, we analyzed the ThT time traces of individual cells by aligning each of the time trace to the frame where the ThT intensity reaches 1,000 au (arbitrary unit), shown as a dashed horizontal gray line in Figure 1D. This alignment revealed a finite increase rate of fluorescence signal (Figure 1E). On the contrary, the length of time it takes to reach mother-cell lysis varies substantially among cells (Figure 1E; the time traces after mother-cell lysis are highlighted in red). On average, after the ThT value reaches 1,000 au, it takes 3.3 h for the spores to be released from mother cells with a standard deviation of 1.4 h (Figures S5 and S6). As a consequence of the finite gradual increase and heterogeneous timing of "exit," different cells reach the different level of peak ThT intensities; the longer the forespore persists in the mother cells the greater the ThT accumulation becomes on forespores. The peak ThT intensity levels are, however, only weakly correlated with the intensity levels on the released endospores (Figure S7). This suggests that not only the negative surface potential of forespores but also the internal environment of mother cells may also

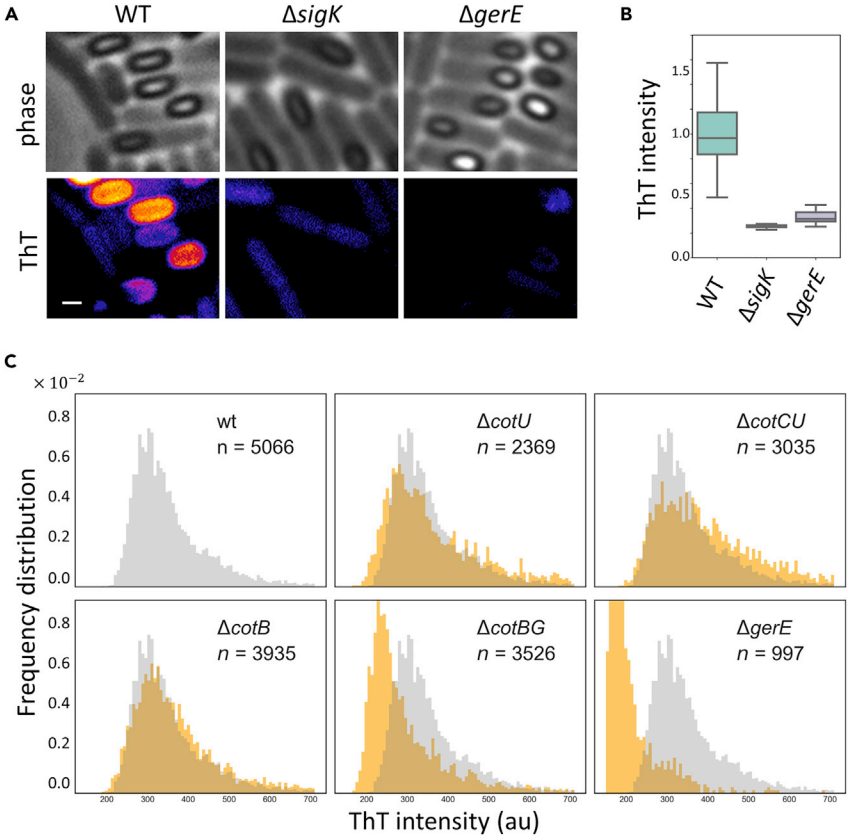

Figure 2. ThT Accumulation Is due to the Negative Surface Potential of Spores

(A) ThT fluorescence images with mutant strains lacking spore coats. Microscopy images of phase contrast (upper panels) and ThT fluorescence (lower panels) of wild-type (wt), *ΔsigK*, and *ΔgerE* strains. Scale bar, 1 μm.

(B) Box and whisker plot showing peak ThT intensities in wt, *ΔsigK*, and *ΔgerE* strains. Thirty cells were analyzed for each strain from two independent experiments. The boxes and whiskers show IQR (interquartile range) and 1.5x IQR, respectively.

(C) Histogram of ThT intensities on endospores with wt, *ΔcotU*, *ΔcotC*, *ΔcotB*, *ΔcotBG*, and *ΔgerE*. The number of endospores analyzed from at least two independent experiments is indicated in each panel. Histogram of wt strain is shown in gray in all panels for comparison with mutant strains (shown in orange). *ΔcotBG* and *ΔgerE* strains exhibit 13.5% and 43% reduction of average ThT intensity levels from wt.

contribute to the accumulation of ThT on forespore periphery. Altogether, our single-cell analysis revealed that the mother-cell-side surface of outer forespore membranes increasingly becomes negative during late sporulation. This conclusion is consistent with the previous study reporting the negative surface potential of mature endospores (ζ potential = −26 mV at pH 7.0) (Piktel et al., 2017).

Outer Spore Coat Accumulates Positive Molecules on the Forespore Surfaces by Electrostatic Attraction

The negative surface potential of developed endospores was implicated with the outer protective layers (Pesce et al., 2014). Therefore, we hypothesized that assembly of outer protective layers (mother-cell side of outer spore membrane) accounts for the negative surface potential of forespores. To examine this conjecture, we measured the ThT dynamics with mutant strains lacking the outer spore coat; specifically, we utilized two deletion mutant strains lacking *sigK* and *gerE*. These genes encode late sporulation regulators, which control the expression of coat proteins and cortex synthesis enzymes. The fluorescence intensities on forespores in these mutant strains were clearly lower than in the wild-type strain (Figures 2A and 2B, see also Figure S4C). Furthermore, time-lapse microscopy with *cotE* deletion strain showed diminished fluorescence intensity increase (Figure S8). These results suggest that the outer layers of forespores are the main contributor to the accumulation of positive ions on the forespore surfaces.

To further examine the contribution of individual coat proteins, we measured ThT fluorescence with the mutants lacking the structural proteins of the outer spore coat. Specifically, we measured ThT intensities on endospore surfaces with the mutant strains of *cotB*, *cotBG*, *cotU*, and *cotCU*, as well as the *gerE* strain. The mutants mostly showed a similar intensity level of ThT compared with wild-type; however, a slight decrease in ThT intensity was observed with the *cotBG* double deletion strain (Figure 2C). Therefore, the negative surface potential of forespores is likely associated with the multiple components of outer endospores coat, including CotB and CotG. Taking into account the previous studies reporting the negative electric charge of endospores (Pesce et al., 2014; Piktel et al., 2017), our results suggest that the outer protective layers of forespores attract cations as forespores develop into resilient spores on the mother-cell side of outer forespore membranes.

Electrostatic Attraction of Cations on Forespore Surfaces Correlates with the Probability of Premature Germination

We next wondered if the cation accumulation on the forespore surface has a biological role in sporulation. Our single-cell time-lapse microscopy showed that some phase-bright forespores turned into phase-dark while still inside mother cells (Figure 3A; upper panel, Figure 3B and Video S4). This change in the phase contrast was reminiscent to the germination of endospores. We thus speculated that this change is due to premature germination within mother cells. To test this idea, we conducted time-lapse microscopy with the mutant strain lacking *gerA* gene, which encodes a main germinant receptor essential for the L-alanine-induced germination. As expected, the deletion of *gerA* gene eliminates the change of phase brightness with forespores (Figure 3A; lower panel, Figure 3B and Video S5). This observation later appeared complementary to the genetic analyses of a recent paper (Ramírez-Guadiana et al., 2017b). Through extensive genetic analysis, this study by Ramirez-Guadiana et al elegantly demonstrated that GerA-mediated premature germination is coupled with morphogenetic errors. However, how cells are able to couple premature germination with a range of different types of morphogenetic errors, such as synthesis of the endospore protective layers (coat and cortex) and core dehydration, remained unclear. We thus aimed to understand the possible mechanism by which the probability of premature germination is tuned during sporulation.

By taking advantage of time-lapse single-cell imaging, we quantified the time evolution of premature germination events. Our data revealed that the probability of premature germination decreases as the level of cation accumulation on the forespore surface increases (Figure 3C). Therefore, we hypothesized that the accumulation of cationic ions on forespore surfaces may prevent the germination of forespores (Figure 3D). Intriguingly, high levels of various cationic ions (e.g., K^+, Na^+, and Ca^{2+}) prevent the germination of "*endo-*"spores by limiting the access of L-alanine to the intermembrane space where the germinant recognition sites of GerA exist (Nagler and Moeller, 2015). Inspired by this, we hypothesized that the electrical polarization of the forespore surfaces relates with the membrane transport across the outer membrane, which alters the probability of premature germination. To identify which native cations may be involved in the modulation of premature germination probability, we used fluorescent indicators APG-2 AM and ANG-2 AM to measure K^+ and Na^+, respectively (Prindle et al., 2015). Both K^+ and Na^+ appeared to be accumulated on forespore periphery regions (Figures S9 and S10). APG-2 provides a clear signal, whereas the other two reporters are relatively noisy with our experimental setting. Therefore, although we emphasize that we do not exclude the possibilities that other cations (e.g., Mg^{2+} or Na^+) are also accumulated, we concluded that K^+ is one of the cations that accumulates highly on the forespore surfaces.

The Premature Germination Probability Can Be Modulated by Chemical Perturbations

To further investigate the hypothesis that the electrical polarization of forespore surfaces suppresses premature germination, we established a minimalistic phenomenological model describing the cation dynamics in cytoplasm (C_c) and forespore-bound (C_f) (Figure 3D). Accounting for the development of negative surface potential of forespores, we assumed that the affinity of cations to forespore surfaces (k_1) increases over time and eventually saturates at a value, k_{1max}. Numerical simulations of this model showed that C_f decreases in a monotonic manner when cation accumulation is inhibited (lower k_{1max}) or cation efflux is increased (higher k_{-2}) (Figure 3E).

We first examined the prediction from the model regarding the decrease in cation accumulation (lower k_{1max}). By taking into account the charge conservation law, it is expected that exogenous cations should act as a competitive inhibitor for native cations (e.g., K^+) in terms of forespore surface accumulation. In

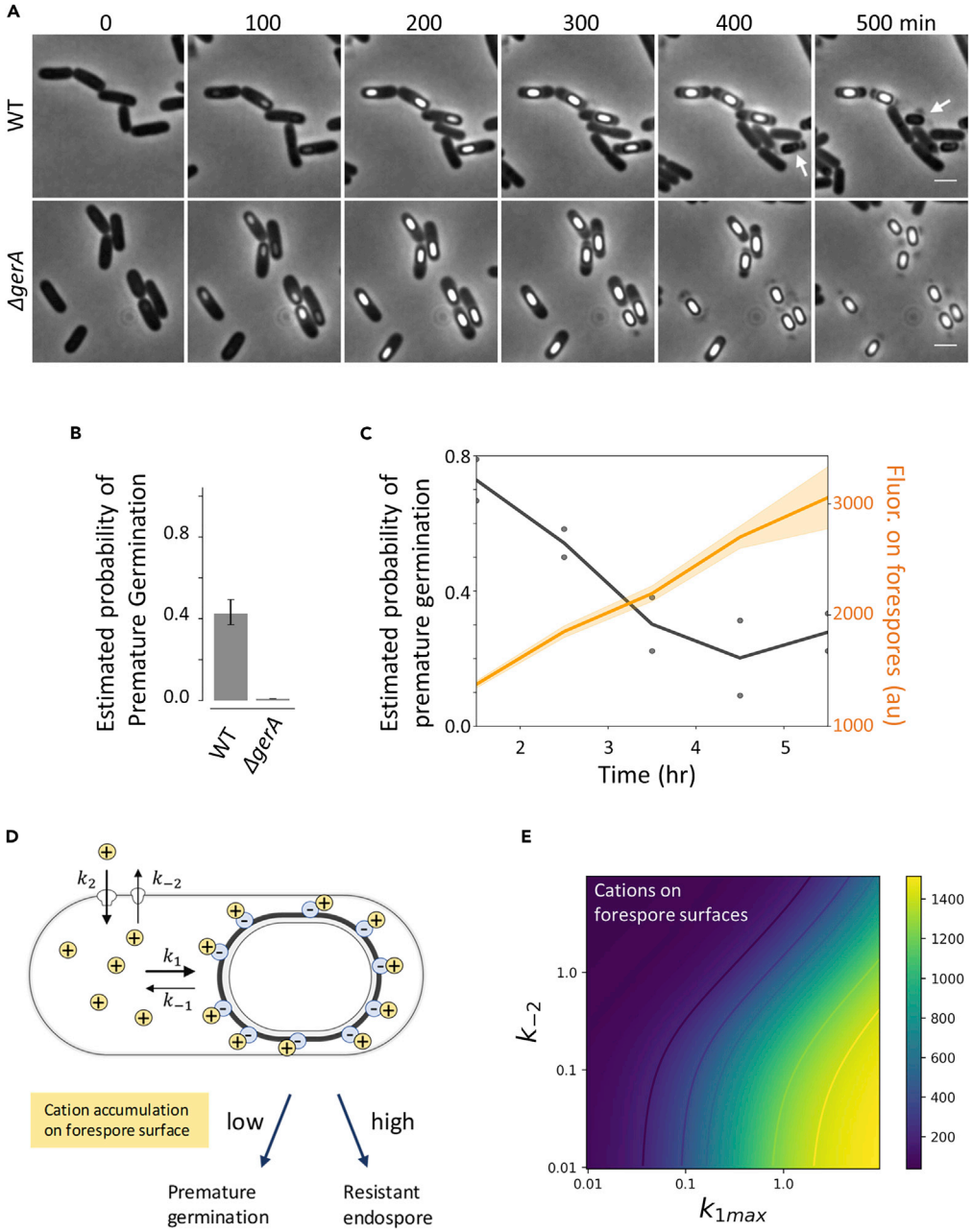

Figure 3. Cation Accumulation on Forespore Surfaces Suppresses Premature Germination

(A) Phase-contrast images of wild-type (WT) and *ΔgerA* strains during sporulation. Scale bar, 2 μm. Premature germination is indicated by white arrows, whereas it is absent with *ΔgerA*.

(B) Estimated probability of premature germination in wt and *ΔgerA* strains (at least 351 sporulating cells were analyzed for each strain from two independent experiments). Error bars are 95% confidence intervals for Poisson distribution.

(C) The probability of premature germination and ThT fluorescence (mean ± SEM) over time. Time series of single-cell ThT intensity are aligned as in Figure 1E, and probability of premature germination was calculated for each hour.

(D) A diagram showing the hypothesis that premature germination probability is coupled with the cation accumulation on forespore surfaces. A phenomenological mathematical model was developed accounting the influx and efflux of cations (k_2 and k_{-2}) and the binding and unbinding of cations to forespore surfaces (k_1 and k_{-1}).

(E) Heatmap showing the simulation results of C_f (cations on forespore surface) computed with various k_{1max} and k_{-2}.

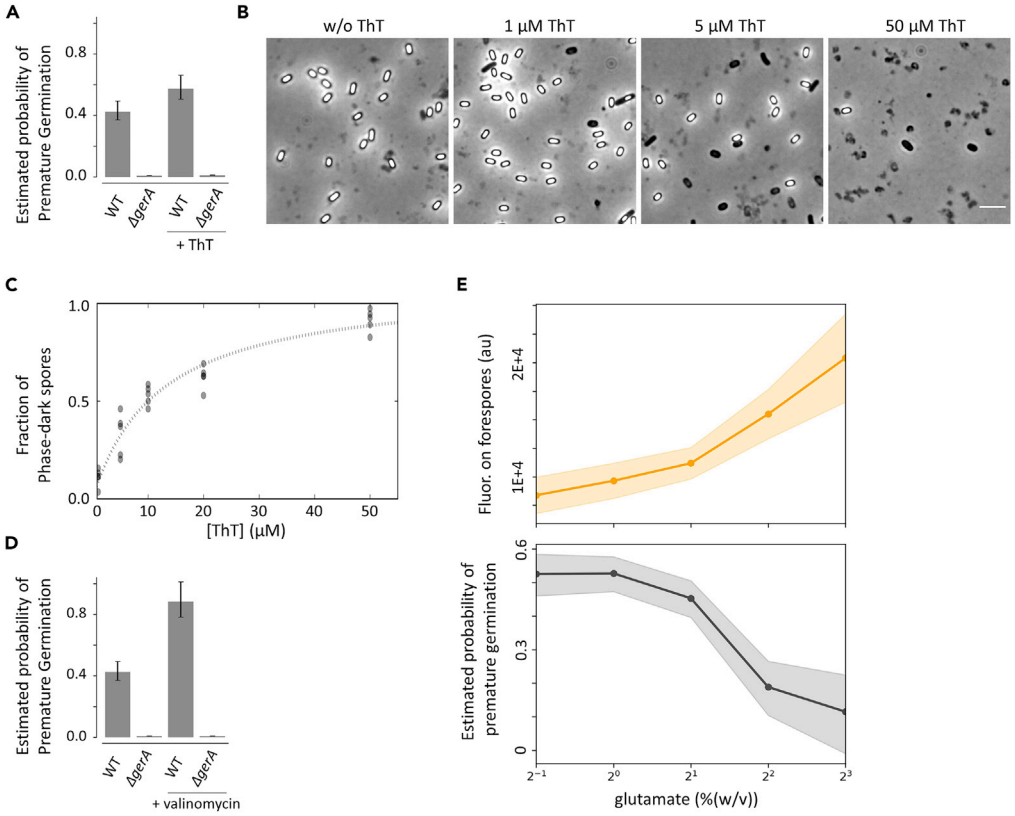

Figure 4. Chemical Perturbations Alter the Probability of Premature Germination

(A) The probability of premature germination with and without ThT. The premature germination remains absent with gerA deletion strain. At least 351 sporulating cells from two independent experiments were analyzed for each condition/strain. The error bars are 95% confidence intervals for Poisson distribution.

(B) Microscopy images of endospores cultured in liquid RM supplemented without or with ThT at 1, 5, and 50 μM. Scale bar, 5 μm. Phase-dark spores are distinguished from vegetative cells by their size.

(C) Quantification of panel (B). The fraction of germinated (phase-dark) endospores increases with increasing ThT.

(D) Addition of valinomycin to the media increases the probability of premature germination. At least 339 sporulating cells were analyzed for each strain/condition. Error bars represent 95% confidence intervals for Poisson distribution.

(E) The peak fluorescence signal on forespore surfaces (TMRM) and the probability of premature germination drops (lower plot) were plotted with various levels of glutamate (final concentrations). Thirty-one cells from three independent experiments were analyzed for each condition. Shaded regions are standard deviation for the upper plot and Poisson confidence intervals for the lower plot.

fact, we observed decreased accumulation of K^+ on forespore surfaces when ThT is present (Figure S9), suggesting that ThT may act as a competitive inhibitor for the cation accumulation. Therefore, our model predicted that addition of ThT should increase the premature germination probability. We estimated the probability of premature germination with and without ThT and found that a greater fraction of forespores, albeit slightly, germinate prematurely when ThT is supplemented to the media (Figure 4A). We confirmed that the premature germination remains absent in *ΔgerA* strain with or without the presence of ThT (Figure 4A). We also examined whether ThT has a direct interaction with the GerA receptor, by conducting germination assay with purified endospores. The result showed that, unlike premature germination of forespores, the germination of mature endospores is unaffected by ThT (Figure S11). This result indicates that the observed increase of premature germination probability is not due to direct interaction between GerA receptor and ThT. To examine the causality of the ThT effect, we tested different ThT concentrations and measured the premature germination probability. The results showed a clear increase of phase-dark endospore fraction as a function of ThT concentrations (Figures 4B and 4C).

We next examined the prediction from the model regarding the increase in cation efflux (higher k_{-2}) by utilizing valinomycin. Valinomycin is a potassium ionophore, which means it increases the membrane

permeability of K^+, leading to a greater k_{-2}. As can be seen in Figure 3E, the model predicts that valinomycin should increase the probability of premature germination. To minimize the potential global impacts of valinomycin, we exposed cells to valinomycin only after cells reached the commitment stage (cultured in the Resuspension Medium [RM] for 3.5 h). Quantification of single-cell time-lapse microscopy data showed that the probability of premature germination significantly increases by valinomycin (Figure 4D). To check that this is not due to a general toxic effect of valinomycin, committed cells of *ΔgerA* strain were also exposed to valinomycin. Contrary to the results with wild-type, the sporulation of the *ΔgerA* strain was unaffected by valinomycin and phase-bright endospores were produced normally (Figures 4D and S12). This result indicates that the crucial role of the transmembrane electrochemical gradient of K^+ during late sporulation (stage IV-VI) is to prevent premature germination and not to support harvesting the energy required for the completion of late sporulation process.

Glutamate Availability Influences the Probability of Premature Germination

Although a previous study suggested that the probability of premature germination may be constant in different media (Ramírez-Guadiana et al., 2017b), our model predicted that environmental conditions that affect the mother-cell membrane potential should alter the probability of premature germination. To this end, we focused on glutamate availability because glutamate is a gating molecule for the K^+ channels (Liu et al., 2017; Prindle et al., 2015). Thus, according to Figure 3E, our model predicted that the premature germination probability would decrease as a function of glutamate levels in the media (lower k_{-2}).

To test this experimentally, cells committed to sporulation were transferred to the RM containing different levels of monosodium glutamate (final concentrations, 0.5–8.0% [w/v]). Then, the probability of premature germination and the forespore-surface charge were determined by single-cell microscopy (Figure 3B). The results showed that, as predicted by the model, the probability of premature germination decreases as a function of glutamate concentrations, whereas the accumulation of charge is inversely correlated with the glutamate levels (Figure 4E). This result indicates that the probability of premature germination is indeed dependent on the media compositions.

Altogether, our results suggested that, under favorable conditions (e.g., high glutamate concentrations in the media), the probability of premature germination is lower. However, when conditions are not favorable (which results in higher k_{-2}) or when forespores have morphological errors (which results in lower k_1), forespores are more prone to germinate prematurely.

Spores Produced in Media Containing ThT Are less Resistant against Wet Heat

Considering that the quality/quantity control of endospores poses a challenge in our society (Nguyen Thi Minh et al., 2011), we wondered if the aforementioned understanding enables us to propose a way of controlling the quality and quantity of endospores.

SpoVV is a concentrative nucleoside transporter that translocates dipicolinic acid (DPA; pyridine-2,6-dicarboxylic acid) against the concentration gradient across the outer forespore membrane from the mother-cell compartment to the intermembrane space (Ramírez-Guadiana et al., 2017a). The deletion of *spoVV* dramatically increases the probability of premature germination (Ramírez-Guadiana et al., 2017b). The reduction of DPA accumulation into spore core is typically associated with wet-heat resistance. We speculate that ThT treatment during sporulation could reproduce the phenotype of the *spoVV* deletion.

To test this, we prepared endospores using the sporulation media RM with and without 10 μM ThT and conducted the wet-heat resistance assays at 80°C for 30 min (Figure 5A). As a control, we also treated endospores with ThT after completion of spore formation (Figure 5A; middle). The survivability of endospores was measured for each sample and normalized to the survivability of endospores prepared without ThT (Figure 5A; top). The endospores exposed to ThT after completing sporulation (Figure 5A; middle) exhibit the survivability comparable with that of the endospores without ThT (Figure 5B). However, the endospores prepared with ThT are more sensitive to the wet-heat treatment than the endospores prepared without ThT (Figure 5B). This result suggests that supplementation of ThT not only reduces the yield of endospores (Figure 4B) but also diminishes the wet-heat resistance property (Figures 5B and 5C).

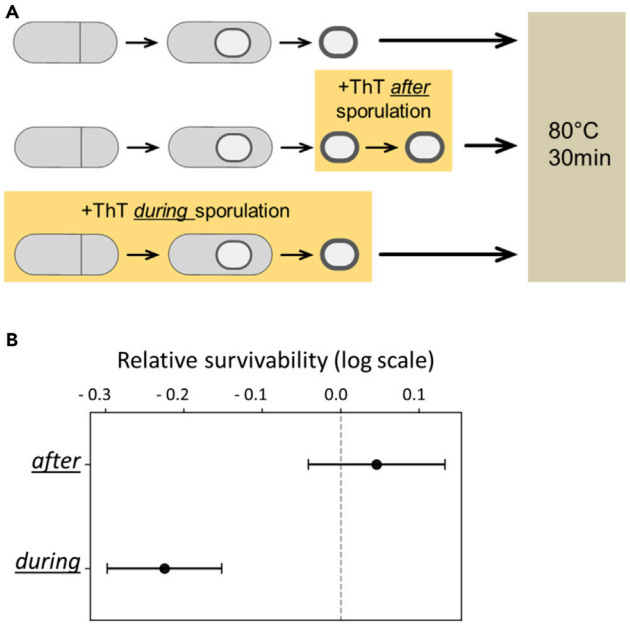

Figure 5. ThT Decreases the Wet-heat Resistance Level of Endospores

(A) Diagram describing the wet-heat resistance assay shown in panel (B). Cells were committed to sporulation (culture for 3.5 h in RM), then moved to RM with and without ThT. Spores were treated at 80°C for 30 min. See Methods for details. (B) Survivability of endospores relative to spores produced without ThT. Wet-heat survivability is lower when spores are formed in the presence of 10 μM ThT. Survivability is comparable when ThT is added to the endospores already prepared in RM without ThT. Error bars are 95% confidence intervals for Poisson distribution based on the number of spores observed. Data from three technical replica and three independent biological replicates.

DISCUSSION

By measuring the cation dynamics during late sporulation, we demonstrated that forespores poorly accumulating cations preferentially germinate while still inside the mother cells. Our results revealed that the premature germination process is coupled with the external and internal conditions during late sporulation through the cation accumulations on forespore surfaces. More specifically, environmental factors affect the cytoplasmic cation levels and the establishment of protective layers and molecule transport across outer membranes alter the accumulation of cations. This mechanism could add plasticity to the genetically regulated processes of sporulation.

Cation Accumulation as an Integrative Indicator for Various Internal and External Environments

A universal challenge of quality control is to integratively monitor the diverse internal and environmental factors that may be influential for the offspring survival. This is a challenging task to be achieved by specific sensor proteins because it requires a wide variety of sensors and integration of inputs. In the case of *B. subtilis* sporulation, our data suggested that the cation accumulation enables coupling of internal and external conditions with the quality control system via premature germination. This mechanism presents an elegant solution to the challenge of sensing diverse environmental factors and morphological errors. This finding also raised the possibility that concentrations of cations may influence the assembly of protective layers, which can result in phenotypic plasticity. It would be interesting to experimentally examine this possibility. Another important unanswered question is the driving force of SpoVV transporter. If the asymmetric surface potential across the outer membrane contributes to the driving force for SpoVV, it may be expected that it is an antiporter. Biophysically analyzing the SpoVV transporter to examine the direction of ion flux and its driving force will be an important topic of research.

Our results suggest that K^+ is an important cation accumulated on forespore surfaces. However, it remains unclear if the accumulation of other cation species (e.g., Na+) is equally or more crucial for the premature germination control. Since various cations are shown to suppress endospore germination (Nagler et al.,

2014), it is conceivable that accumulation of different ion species may have different impacts to assembly of coat proteins.

Potential Roles of Premature Germination in Biofilm Colonies

Our study presents a perspective in the emerging research field of bacterial electrical signaling (Lee et al., 2017). We showed that the probability of premature germination depends on the mother cells' ability to take up cations from their environment. Because the efficiency of cation uptake can be altered by the biofilm electrical signaling (Prindle et al., 2015), electrical signaling should, in theory, alter the probability of premature germination. Intriguingly, in *B. subtilis* biofilms, sporulation is regulated both in space and time (Branda et al., 2001). However, the mechanism by which this pattern emerges remains unclear. Based on the insight we gained in this study, we suspect that the spatiotemporal organization of sporulation during biofilm formation may also be regulated by electrical signaling and premature germination. Cell lysis after premature germination may also provide some benefits to the surrounding cells by providing nutrients or physical space. Such interactions would be pronounced when cells are structurally organized, such as in biofilms (Asally et al., 2012; Momeni et al., 2013). Hence, it is plausible to speculate that cell death through premature germination may provide more significant population-level impacts in biofilms. In our future research, we shall determine the potential roles of biofilm electrical signaling to sporulation, and *vice versa*.

ThT as a Potential Chemical to Prevent the Formation of Resistant Endospores

We showed that ThT decreases the yield of endospores by promoting the premature germination, while at the same time lowering the wet-heat resistance of endospores. These results propose a usage of ThT as an agent to limit the formation of resistant endospores. We believe this is an attractive possibility since ThT is likely non-toxic to humans. Intriguingly, ThT at 50 μM has been shown to prevent the disruption of muscle sarcomeres during aging and extend the median lifespan of *C. elegans* (Alavez et al., 2011). Coincidentally, 50 μM is the ThT concentration at which we observed almost complete abolishment of phase-bright endospore formation. Therefore, ThT at a concentration around 50 μM may bring multiple benefits to the industries where endospore formation poses problems. We also note that ThT is a relatively inexpensive chemical; a liter of 50 μM ThT solution would cost approximately 0.05 US dollars. Bacterial spores of other species are also negatively charged (Pesce et al., 2014; Piktel et al., 2017), which suggests that the mechanism may be conserved among species. As such, systematic investigation of the impact of ThT in various spore-forming bacterial species, such as *B. anthrax* and *C. difficile*, would be an important avenue of further research.

Limitations of the Study

The exact molecular mechanisms by which premature germination is coupled with cation accumulation remain unclear. Additional experiments are needed to quantitatively determine the electrical potential across outer and inner spore membranes and to understand their roles in sporulation and germination. Physicochemical modeling framework is still to be done to understand the electrical potential dynamics during sporulation.

METHODS

All methods can be found in the accompanying Transparent Methods supplemental file.

SUPPLEMENTAL INFORMATION

Supplemental Information can be found online at https://doi.org/10.1016/j.isci.2019.05.044.

ACKNOWLEDGMENTS

We thank GM Süel, P Schäfer, DY Lee, T Çağatay, A Kuchina, A Saggese, and the members of the Asally laboratory (J Stratford, M Delise, I Lopez-Grobas, and C Edwards) for their comments to the drafts of the manuscript; the anonymous reviewers for constructive criticism; E Ricca, L Baccigalupi, and R Isticato for generously providing bacterial strains; and the reviewers for their constructive criticisms. This study was supported by the start-up fund from University of Warwick, SLS Pump priming fund, and the Royal Society Research Grant to M.A., BBSRC/EPSRC grant to WISB (BB/M017982/1), and the Spanish Ministry of Economy and Competitiveness and FEDER (FIS2015-66503-C3-1-P) and the Maria de Maeztu Program for Units of Excellence (project MDM-2014-0370) to J.G.-O. J.M.B. acknowledges the funding by the

MRC Doctoral Training Partnership (MR/N014294/1). P.B. was supported by a scholarship from the Region Auvergne-Rhone-Alpes and the Université Grenoble Alpes.

AUTHOR CONTRIBUTIONS

T.S. and P.B. prepared samples for experiments and conducted experiments. T.S. and M.A. designed experiments and analyzed experimental data. J.M.B. analyzed the data and electrochemical models. J.G.-O. developed theoretical formalism and performed numerical simulations. M.A. wrote the manuscript with input from all other authors. All authors provided critical feedback to the manuscript and discussed the results.

DECLARATION OF INTERESTS

The authors declare no competing interests.

Received: August 23, 2018
Revised: December 18, 2018
Accepted: May 30, 2019
Published: June 28, 2019

REFERENCES

Alavez, S., Vantipalli, M.C., Zucker, D.J.S., Klang, I.M., and Lithgow, G.J. (2011). Amyloid-binding compounds maintain protein homeostasis during ageing and extend lifespan. Nature *472*, 226–229.

Asally, M., Kittisopikul, M., Rue, P., Du, Y., Hu, Z., Cagatay, T., Robinson, A.B., Lu, H., Garcia-Ojalvo, J., and Suel, G.M. (2012). Localized cell death focuses mechanical forces during 3D patterning in a biofilm. Proc. Natl. Acad. Sci. U S A *109*, 18891–18896.

Branda, S.S., Gonzalez-Pastor, J.E., Ben-Yehuda, S., Losick, R., Kolter, R., González-Pastor, J.E., Ben-Yehuda, S., Losick, R., and Kolter, R. (2001). Fruiting body formation by *Bacillus subtilis*. Proc. Natl. Acad. Sci. U S A *98*, 11621–11626.

Bruni, G.N., Weekley, R.A., Dodd, B.J.T., and Kralj, J.M. (2017). Voltage-gated calcium flux mediates *Escherichia coli* mechanosensation. Proc. Natl. Acad. Sci. U S A *114*, 9445–9450.

Driks, A. (1999). *Bacillus subtilis* spore coat. Microbiol. Mol. Biol. Rev. *63*, 1–20.

Eijlander, R.T., Abee, T., and Kuipers, O.P. (2011). Bacterial spores in food: how phenotypic variability complicates prediction of spore properties and bacterial behavior. Curr. Opin. Biotechnol. *22*, 180–186.

Eijlander, R.T., De Jong, A., Krawczyk, A.O., Holsappel, S., and Kuipers, O.P. (2014). SporeWeb: an interactive journey through the complete sporulation cycle of *Bacillus subtilis*. Nucleic Acids Res. *42*, 685–691.

Humphries, J., Xiong, L., Liu, J., Prindle, A., Yuan, F., Arjes, H.A., Tsimring, L., and Süel, G.M. (2017). Species-Independent attraction to biofilms through electrical signaling. Cell *168*, 200–209.e12.

Kralj, J.M., Hochbaum, D.R., Douglass, A.D., and Cohen, A.E. (2011). Electrical spiking in *Escherichia coli* probed with a fluorescent voltage-indicating protein. Science *333*, 345–348.

Kuchina, A., Espinar, L., Çağatay, T., Balbin, A.O., Zhang, F., Alvarado, A., Garcia-Ojalvo, J., and Süel, G.M. (2011). Temporal competition between differentiation programs determines cell fate choice. Mol. Syst. Biol. *7*, 1–11.

Lee, D.D., Galera-Laporta, L., Bialecka-Fornal, M., Moon, E.C., Shen, Z., Briggs, S.P., Garcia-Ojalvo, J., and Süel, G.M. (2019). Magnesium flux modulates ribosomes to increase bacterial survival. Cell *177*, 352–360.e13.

Lee, D.D., Prindle, A., Liu, J., and Süel, G.M. (2017). SnapShot: electrochemical communication in biofilms. Cell *170*, 214–214.e1.

Liu, J., Martinez-Corral, R., Prindle, A., Lee, D.D., Larkin, J., Gabalda-Sagarra, M., Garcia-Ojalvo, J., and Süel, G.M. (2017). Coupling between distant biofilms and emergence of nutrient time-sharing. Science *356*, 638–642.

Liu, J., Prindle, A., Humphries, J., Gabalda-Sagarra, M., Asally, M., Lee, D.D., Ly, S., Garcia-Ojalvo, J., and Süel, G.M. (2015). Metabolic co-dependence gives rise to collective oscillations within biofilms. Nature *523*, 550–554.

Lo, C.J., Leake, M.C., Pilizota, T., and Berry, R.M. (2007). Nonequivalence of membrane voltage and ion-gradient as driving forces for the bacterial flagellar motor at low load. Biophys. J. *93*, 294–302.

Lopez-Garrido, J., Ojkic, N., Khanna, K., Wagner, F.R., Villa, E., Endres, R.G., and Pogliano, K. (2018). Chromosome translocation inflates *Bacillus* forespores and impacts cellular morphology. Cell *172*, 758–770.e14.

Mao, L., Jiang, S., Wang, B., Chen, L., Yao, Q., and Chen, K. (2011). Protein profile of *Bacillus subtilis* spore. Curr. Microbiol. *63*, 198–205.

Momeni, B., Waite, A.J., and Shou, W. (2013). Spatial self-organization favors heterotypic cooperation over cheating. Elife *2*, e00960.

Mutlu, A., Trauth, S., Ziesack, M., Nagler, K., Bergeest, J.P., Rohr, K., Becker, N., Höfer, T., and Bischofs, I.B. (2018). Phenotypic memory in *Bacillus subtilis* links dormancy entry and exit by a spore quantity-quality tradeoff. Nat. Commun. *9*, 69.

Nagler, K., and Moeller, R. (2015). Systematic investigation of germination responses of *Bacillus subtilis* spores in different high-salinity environments. FEMS Microbiol. Ecol. *91*, 1–10.

Nagler, K., Setlow, P., Li, Y.Q., and Moeller, R. (2014). High salinity alters the germination behavior of *Bacillus subtilis* spores with nutrient and nonnutrient germinants. Appl. Environ. Microbiol. *80*, 1314–1321.

Narula, J., Fujita, M., and Igoshin, O.A. (2016). Functional requirements of cellular differentiation: lessons from *Bacillus subtilis*. Curr. Opin. Microbiol. *34*, 38–46.

Narula, J., Kuchina, A., Lee, D.D., Fujita, M., Süel, G.M., and Igoshin, O.A. (2015). Chromosomal arrangement of Phosphorelay genes couples sporulation and DNA replication. Cell *162*, 328–337.

Nguyen Thi Minh, H., Durand, A., Loison, P., Perrier-Cornet, J.-M., and Gervais, P. (2011). Effect of sporulation conditions on the resistance of *Bacillus subtilis* spores to heat and high pressure. Appl. Microbiol. Biotechnol. *90*, 1409–1417.

Palop, A., Mañas, P., and Condón, S. (1999). Sporulation temperature and heat resistance of *Bacillus* spores: a review. J. Food Saf. *19*, 57–72.

Pesce, G., Rusciano, G., Sasso, A., Isticato, R., Sirec, T., and Ricca, E. (2014). Surface charge and hydrodynamic coefficient measurements of *Bacillus subtilis* spore by optical tweezers. Colloids Surf. B Biointerfaces *116*, 568–575.

Piktel, E., Pogoda, K., Roman, M., Niemirowicz, K., Tokajuk, G., Wróblewska, M., Szynaka, B., Kwiatek, W.M., Savage, P.B., and Bucki, R. (2017). Sporicidal activity of ceragenin CSA-13 against *Bacillus subtilis*. Sci. Rep. *7*, 44452.

Plomp, M., Carroll, A.M., Setlow, P., and Malkin, A.J. (2014). Architecture and assembly of the *Bacillus subtilis* spore coat. PLoS One *9*, e108560.

Prindle, A., Liu, J., Asally, M., Ly, S., Garcia-Ojalvo, J., and Süel, G.M.G.M. (2015). Ion channels enable electrical communication in bacterial communities. Nature *527*, 59–63.

Prindle, A., Samayoa, P., Razinkov, I., Danino, T., Tsimring, L.S., and Hasty, J. (2012). A sensing array of radically coupled genetic "biopixels." Nature *481*, 39–44.

Ramírez-Guadiana, F.H., Meeske, A.J., Rodrigues, C.D.A., Barajas-Ornelas, R.D.C., Kruse, A.C., and Rudner, D.Z. (2017a). A two-step transport pathway allows the mother cell to nurture the developing spore in *Bacillus subtilis*. PLoS Genet. *13*, e1007015.

Ramírez-Guadiana, F.H., Meeske, A.J., Wang, X., Rodrigues, C.D.A., and Rudner, D.Z. (2017b). The *Bacillus subtilis* germinant receptor GerA triggers premature germination in response to morphological defects during sporulation. Mol. Microbiol. *105*, 689–704.

Rose, R., Setlow, B., Monroe, A., Mallozzi, M., Driks, A., and Setlow, P. (2007). Comparison of the properties of *Bacillus subtilis* spores made in liquid or on agar plates. J. Appl. Microbiol. *103*, 691–699.

Stratford, J.P., Edwards, C.L.A., Ghanshyam, M.J., Malyshev, D., Delise, M.A., Hayashi, Y., and Asally, M. (2019). Electrically induced bacterial membrane-potential dynamics correspond to cellular proliferation capacity. Proc. Natl. Acad. Sci. U S A *116*, 9552–9557.

Taheri-Araghi, S., Brown, S.D., Sauls, J.T., McIntosh, D.B., and Jun, S. (2015). Single-cell physiology. Annu. Rev. Biophys. *44*, 123–142.

Tan, I.S., Weiss, C.A., Popham, D.L., and Ramamurthi, K.S. (2015). A quality-control mechanism removes unfit cells from a population of sporulating bacteria. Dev. Cell *34*, 682–693.

Wilkinson, B.J., Deans, J.A., and Ellar, D.J. (1975). Biochemical evidence for the reversed polarity of the outer membrane of the bacterial forespore. Biochem. J. *152*, 561–569.

Willis, L., Refahi, Y., Wightman, R., Landrein, B., Teles, J., Huang, K.C., Meyerowitz, E.M., and Jönsson, H. (2016). Cell size and growth regulation in the *Arabidopsis thaliana* apical stem cell niche. Proc. Natl. Acad. Sci. U S A *113*, E8238–E8246.

ISCI, Volume *16*

Supplemental Information

Electrical Polarization Enables Integrative Quality Control during Bacterial Differentiation into Spores

Teja Sirec, Jonatan M. Benarroch, Pauline Buffard, Jordi Garcia-Ojalvo, and Munehiro Asally

Supplementary figures and legends

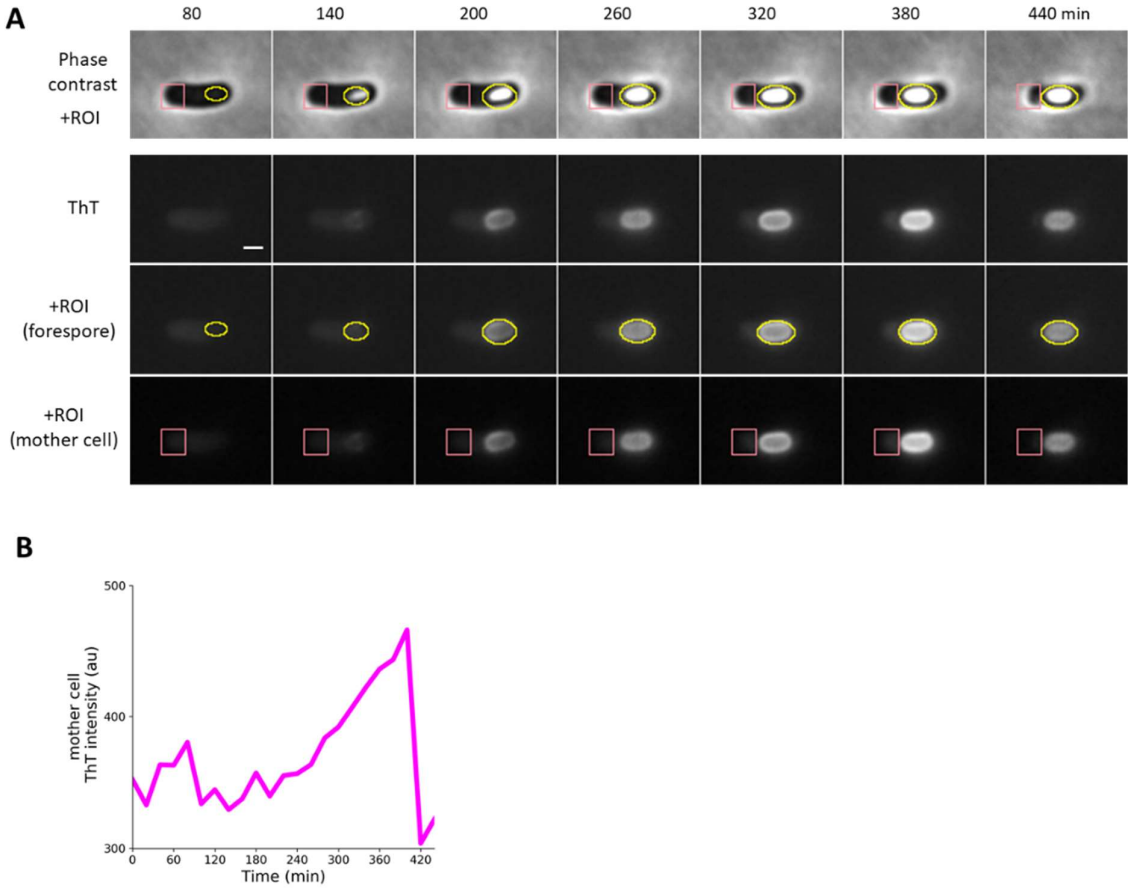

Figure S1. Single-cell image analysis, Related to Figure 1
A) Yellow and Magenta indicate the ROIs (region of interest) used for the intensity measurement on spore and in mother cell, respectively. Images correspond to Figure 1. **B)** ThT intensity over time measured for the mother-cell region (magenta square in panel A).

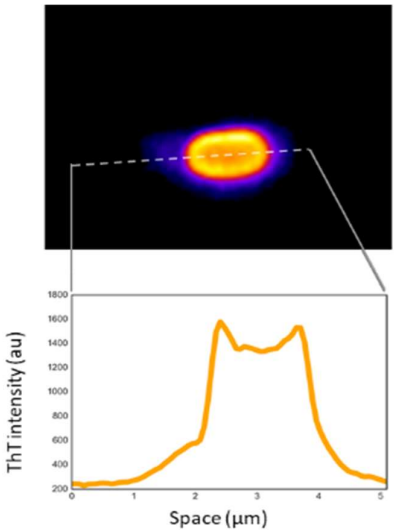

Figure S2. ThT accumulates on the periphery of forespores, Related to Figure 1
ThT fluorescence intensity over the space along the dashed line shown in the image.

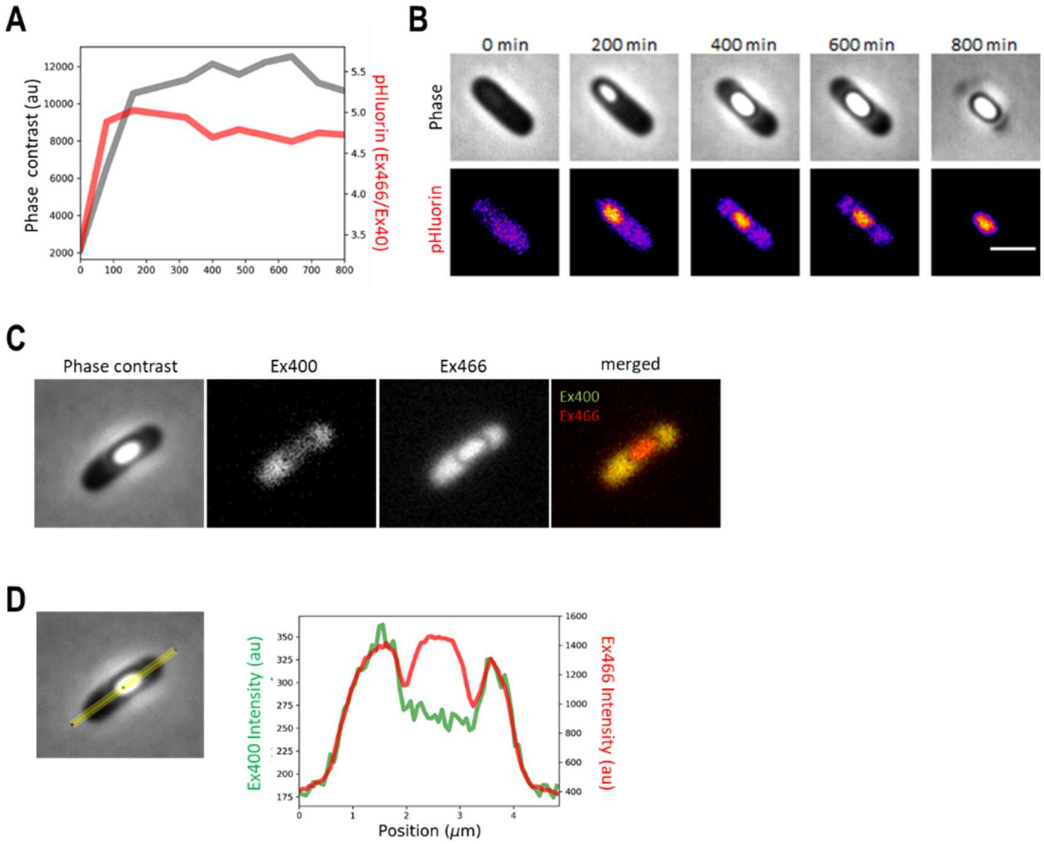

Figure S3. pH dynamics during sporulation, Related to Figure 1

A) Time series of forespore/endospore intensities of phase contrast channel in grey and pHluorin in red (Ex466/Ex400 ratio) in wild type strain. Time series shows a steep acidification of forespore cytoplasm coinciding with the occurrence of phase-bright spore. Time series is representative from five independent experiments. We emphasize that the plateau signal after initial increase does not mean pH is stable. This is because pH may be out of the pHluorin dynamic range. **B)** Film-strip images showing the phase-contrast channel (upper) and pHluorin Ex466/Ex400 ratio (lower). Scale bar, 2 μm. **C)** microscopy images of phase-contrast, Ex400, Ex466 channels and merged image of Ex400 and Ex466. pHluorin is likely excluded from the forespore periphery due to the assembly of coat layers. **D)** Ex400 and Ex466 fluorescence signals from pHluorin were plotted along the yellow line shown.

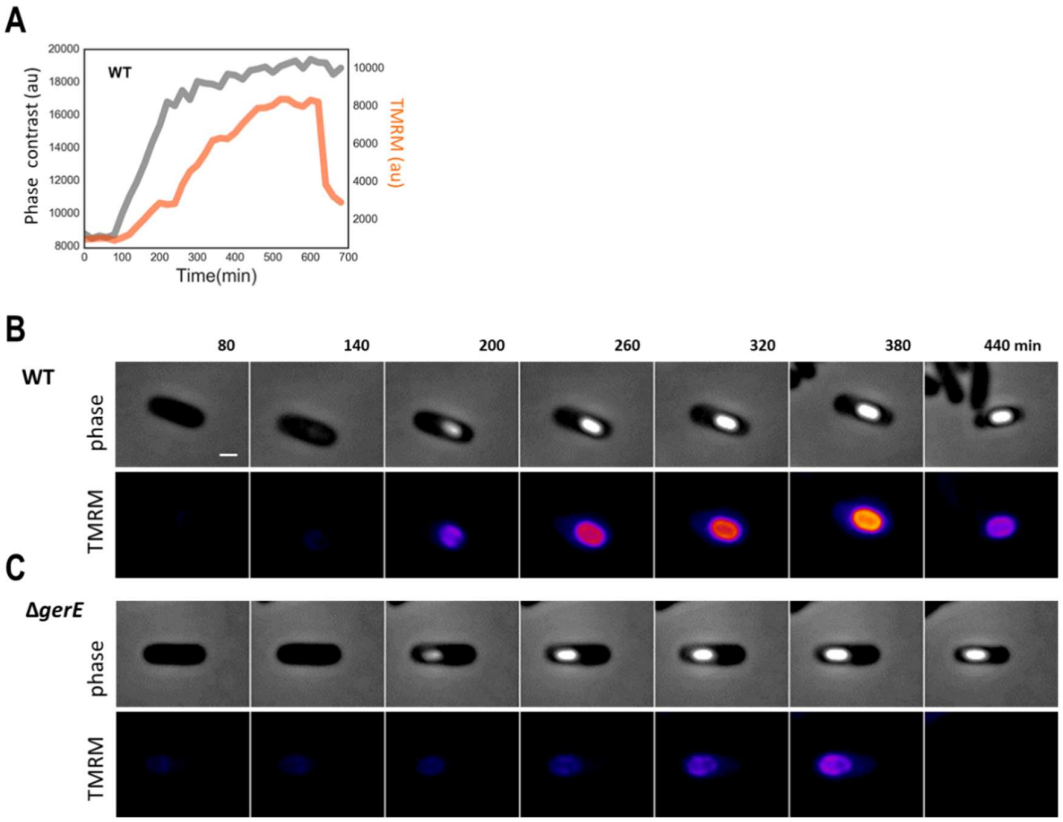

Figure S4. TMRM shows the pattern observed with ThT, Related to Figure 1
A) Time traces of phase-contrast and TMRM fluorescence in spore regions of wildtype strain. **B)** Filmstrip images of phase-contrast and TMRM fluorescence with wildtype strain. The scale bar is 1 μm. **C)** Filmstrip images of phase-contrast and TMRM fluorescence with gerE strain.

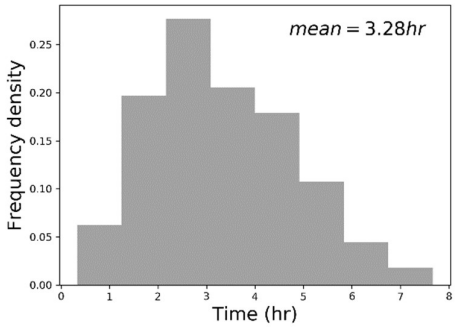

Figure S5. Histogram of the late sporulation duration in presence of ThT, Related to Figure 1
The late sporulation duration here is defined by the time between the ThT intensity reaching 1000 au and mother-cell lysis. 122 sporulating cells from two independent experiments were analyzed.

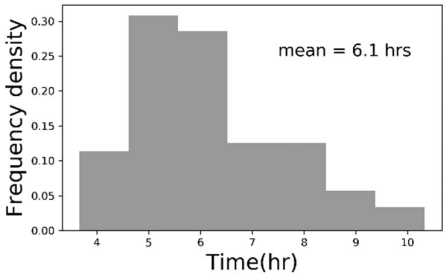

Figure S6. Histogram of the late sporulation duration in absence of ThT, Related to Figure 1
The late sporulation duration defined by the time that phase-contrast intensity started to increase until mother-cell lysis. 101 sporulating cells from three independent experiments were analyzed.

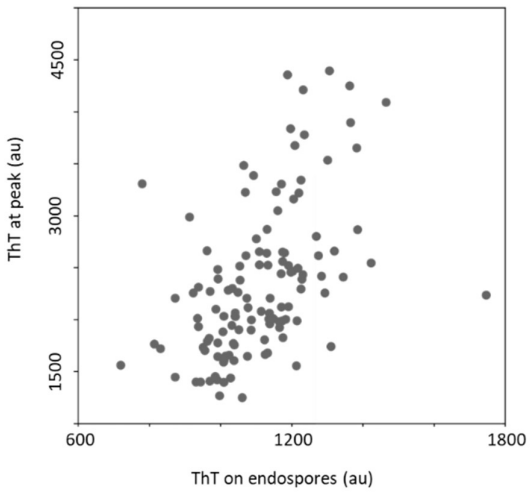

Figure S7. ThT intensity after mother-cell lysis weakly correlates with peak ThT intensity, Related to Figure 1

Scatter plot of ThT intensity after (x-axis) and before (y-axis) mother-cell lysis. The peak ThT intensity was determined by the maximum value of timeseries. 122 sporulating cells from two independent experiments were analyzed.

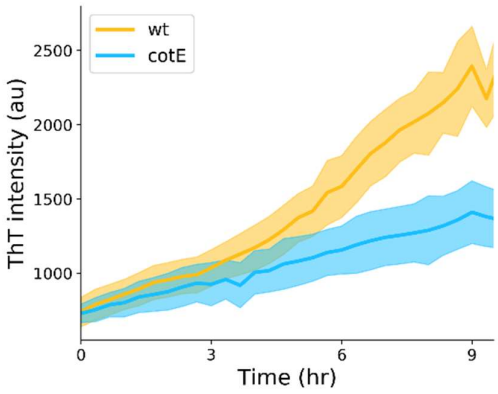

Figure S8. ThT intensity is lower in *cotE* strain, Related to Figure 2
Mean ThT time traces with wildtype and *cotE* strain. 16 wildtype cells and 34 cotE cells from two experiments were analyzed. Shaded show the standard deviations.

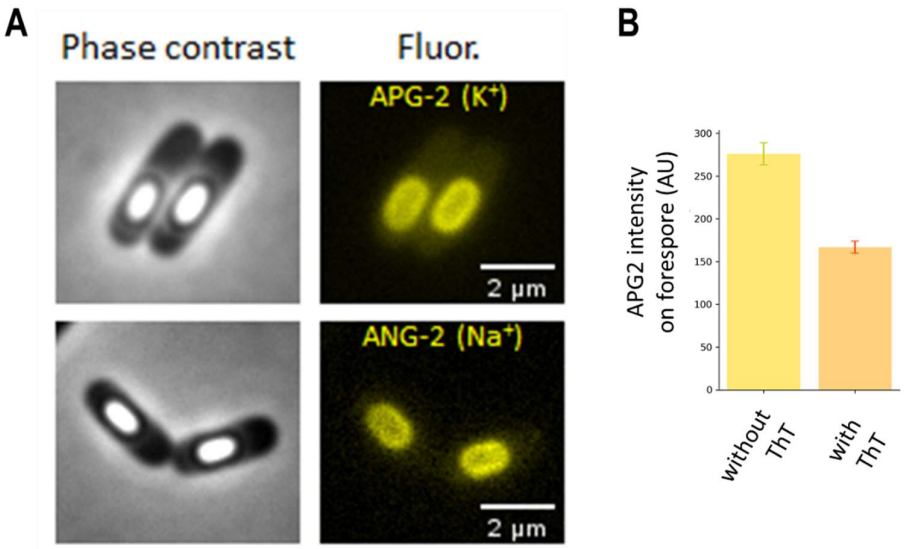

Figure S9. Potassium and sodium accumulate on forespore surfaces, Related to Figure 2
A) Microscopy images show phase contrast (left, grey), and APG2-AM and ANG2-AM fluorescence (right, yellow) on spores. Scale bar, 2 µm.
B) Quantification of APG2-AM fluorescence on forespore with and without ThT. 30 sporulating cells from three independent experiments were analyzed for each condition. Error bars are standard error of mean.

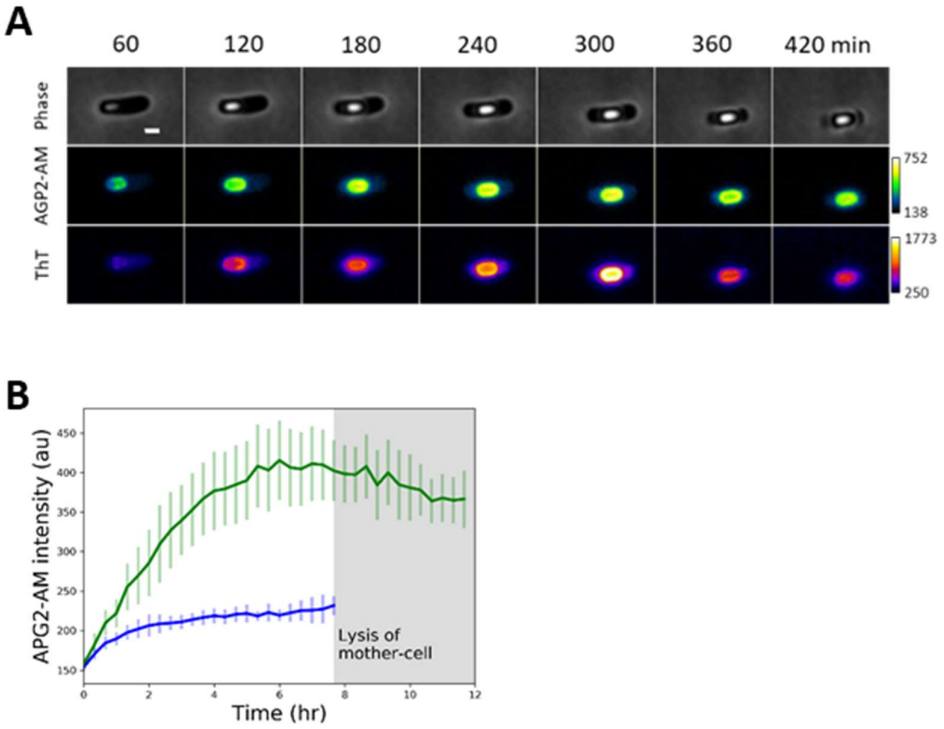

Figure S10. APG2 fluorescence increases on the forespore periphery during sporulation, Related to Figure 2

A) Phase-contrast, APG-2, ThT fluorescence images. Scale bar, 1 μm. B) Time traces of mean fluorescence intensity of APG-2 AM on the forespore regions (green, n = 14) and mother-cell cytosol (blue, n = 10). Post lysis of the mother cell signal is indistinguishable from the background. Error bars are standard deviation.

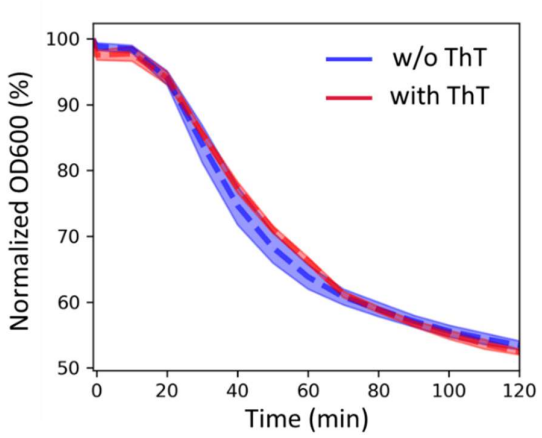

Figure S11. Germination is not affected by ThT, Related to Figure 3
Endospore germination was measured by OD600 after addition of L-alanine with and without ThT (10 μM). Shaded regions are standard deviation. Data obtained with three biological replicas.

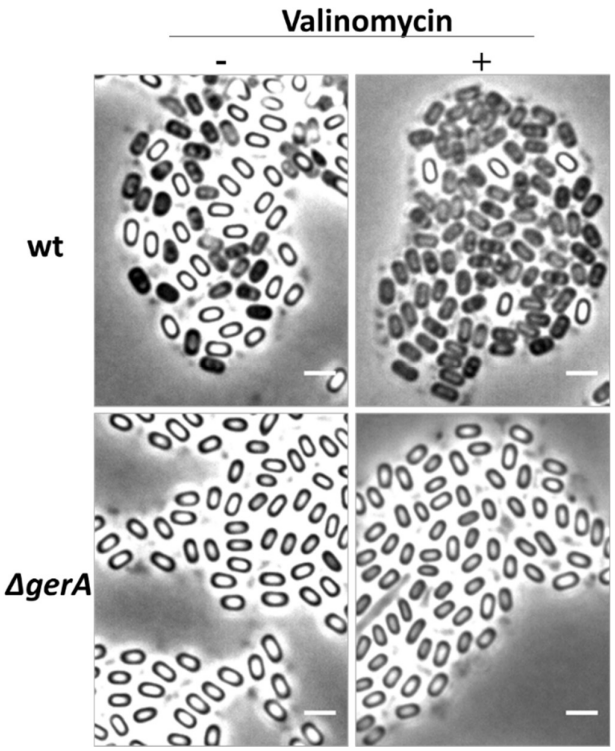

Figure S12. Valinomycin affects sporulation of wild type strain but not of *gerA* mutant, Related to Figure 4

Microscopy images showing representative samples of wild type and *gerA* mutant strain. Phase contrast (grey) images show the proportion of white and black spores without and with valinomycin treatment. Scale bar, 2 μm.

Supplementary movie legends

Movie 1. Dynamics of ThT during sporulation, Related to Figure 1
Fluorescence time-lapse microscopy images corresponding to the main Figure 1B and 1C.

Movie 2. pHluorin dynamics during sporulation, Related to Figure 1
Time-lapse microscopy images showing a sporulating cell in phase contrast (left) and pHluorin (right). The intensity in pHluorin images is the ratio of Ex466/Ex400. Lighter colors indicate low pH and darker colors indicate high pH.

Movie 3. TMRM dynamics during sporulation, Related to Figure 1
Time-lapse microscopy images of a sporulating cell in phase contrast and TMRM fluorescence.

Movie 4. Phase contrast images of live wildtype cells during sporulation, Related to Figure 3
Time-lapse microscopy showing sporulating wildtype cells in phase contrast. Several developing forespores turn phase-dark in the mother cells. Scale bar, 2 µm.

Movie 5. Phase contrast images of *gerA* cells during sporulation, Related to Figure 3
Time-lapse microscopy showing *gerA* sporulating cells in phase contrast. No premature germination was observed with this strain. Scale bar, 2 µm.

Transparent Methods

Growth Conditions and Strain Constructions

The strains of *B. subtilis* and *E. coli* used in this study are listed in Table. All strains were routinely grown in Lysogeny Broth (LB) or LB agar plates at 37 °C. When culturing the strains carrying antibiotic-resistance genes, appropriate antibiotics were supplemented in LB at the concentrations of 100 µg/mL ampicillin, 300 µg/mL spectinomycin, or 5 µg/mL chloramphenicol. All strains and primers used in this study are listed in the Table S1. PY79 *ΔgerA* strain was derived by transforming pTS39 plasmid using the standard one-step *B. subtilis* transformation procedure described previously (Jarmer et al., 2002). For the construction of pTS39 plasmid, the upstream and downstream regions of *gerAA* gene locus are amplified by Polymerase Chain Reaction (PCR) with PrimeSTAR Max DNA Polymerase (Takara) using the primer sets AP233/AP234 and AP237/AP238, respectively. The sequences of these primers, as well as all the other primers used in this study, are listed in Table. The plasmid backbone and spectinomycin-resistance cassette were amplified from pDL30 plasmid (Kuchina et al., 2011) with the primer set AP232/AP239 and AP235/AP236. The PCR products were analyzed by electrophoresis and subsequently purified from agarose gel using gel extraction kit (QIAGEN). The purified DNA fragments were then assembled using the Gibson assembly kit (NEB) and transformed into chemically competent *E. coli* cells (Top10) using the standard heat-shock transformation method. Cells were then plated onto LB agar plates with ampicillin and cultured overnight at 37°C. The colonies obtained were screened by colony PCR using the primer sets AP233/AP238. The plasmids were then extracted from the positive clones and sent for the Sanger sequencing service by the Source BioScience. The resultant sequence data were aligned to the sequence assembly *in silico* using Benchling (benchling.com). Once the sequence is confirmed, pTS39 plasmid was linearized with the restriction enzyme ScaI, and transformed into wildtype PY79. The colonies grown on LB agar plate with spectinomycin were screened by colony PCR using the primer sets AP252/AP149 and AP253/AP3 to check the double crossover homologous recombination. The positive clones were stored in 25 % glycerol at -80 °C.

Time-lapse microscopy of sporulation with Resuspension medium (RM)

The sporulation dynamics of *B. subtilis* cells were observed as previously described (Kuchina et al., 2011), using the fluorescence microscopy Leica DMi8 equipped with an automated stage, Hamamatsu Orca-flash 4.0 scientific CMOS (complementary metal–oxide–semiconductor) camera, and a PeCon incubation system. The objective lens HCX PL FLUOTAR 100x/1.30 OIL PH3 was used for all microscopy assays. ThT fluorescence was detected with 100 ms exposure with Ex438/24 and Em483/32 filters (Semrock). TMRM fluorescence was detected with 300 ms exposure with Ex554/23 and Em609/54 filters (Semrock). APG-2 and ANG-2 were detected with 300 ms exposure with Ex509/22 and Em544/22 filters (Semrock). pHluorin was detected with 300 ms exposure with Ex400/40, Ex466/40 and Em500/24 filters (Semrock). For all experiments, white LED of SOLA-SM II light engine (Lumencor) was used with the power level 10/255 (~4% of full power). For time-lapse microscopy experiments, images were taken every 20 min. For preparation of samples, overnight LB cultures of *B. subtilis* were resuspended in 20 % (v/v) LB at OD_{600} ~ 0.1 and incubated at 37 °C with shaking until reaching OD_{600} 0.6 - 0.8. The cultures were then centrifuged at 4,000 rpm (revolutions per minute) for 10 minutes, and resuspended in equal volume of pre-warmed Resuspension Medium (RM) (Sterlini and Mandelstam, 1969) (RM; composition per 1 liter: 46 µg FeCl2, 4.8 g MgSO4, 12.6 mg MnCl2, 535 mg NH4Cl, 106 mg Na2SO4, 68 mg KH2PO4, 96.5 mg NH4NO3, 219 mg CaCl2, 2 g monosodium L-glutamate), and then incubated for 3 hours at 37°C in a shaking incubator prior to microscopy assay. The cultures were then deposited on LMP (Low Melting Point) agarose pads prepared as described previously (Kuchina et al., 2011). Briefly, 1.8% (weight/volume) LMP agarose was dissolved in RM without glutamate by microwave and left to cool down before adding glutamate. When specified, fluorescent dyes or inhibitors are supplemented to the RM at the following concentrations; 1 µM APG-2 AM (TefLab), 10 µM (unless specified otherwise in the figure legend) Thioflavin T (Sigma-Aldrich), 10 µM valinomycin (Sigma-Aldrich), 20 nM TMRM (Molecular Probes). Working concentrations of these chemicals are determined based on the previous literature (Depauw et al., 2016; Kralj et al., 2011; Prindle et al., 2015; Roder and Hille, 2014). 1 mL of the RM-LMP agarose solution was placed onto a cover glass (22 millimeters by 22 millimeters) and covered by another cover glass of the same

size. Once agarose is polymerized, the coverslip on the top was removed, and 2 µL of cell cultures were deposited onto the agarose pads. The pads were cut and placed in a glass-bottom dish (Willco, HBST-5040) to be used for microscopy assays.

Spore preparation

Sporulation of *B. subtilis* cells was induced by the resuspension method of Sterlini & Mandelstam as described previously (Sterlini and Mandelstam, 1969). A single colony of *B. subtilis* was inoculated in 5 mL LB and incubated for an overnight at 37°C in a shaking incubator (200 rpm). The culture was then diluted to OD_{600} of 0.1 and incubated at 37°C in prewarmed 20% (volume/volume) LB for 3 hours to reach OD_{600} of 0.6 – 0.8. The culture was centrifuged for 10 minutes at 4,000 rpm at room temperature (RT) and resuspended in an equal volume of pre-warmed Resuspension Media (RM). After an overnight incubation in RM at 37°C in a shaking incubator, the culture was centrifuged for 10 minutes at 4,000 rpm and washed 3 times in distilled water. To remove the vegetative cells from the solution, the culture was treated with 100 µg/mL lysozyme in 10mM Tris-HCl (pH 6.8) and incubated for an hour at 37°C with aeration (200 rpm). The resultant solution was subsequently washed in 1M NaCl, milli-Q water, 1M KCl and 10 times in milli-Q water. All the centrifugation steps for washing were performed for 10 minutes at 4,000 rpm at RT. To ensure endospores are purified, the resultant solutions were inspected under microscope using 1.8% (w/v) low-melting-point agarose pad containing PBS. Spores are kept at 4°C and experiments were conducted within a week of spore preparation.

Germination assays

For the germination assay by a spectrophotometer, purified free spores were diluted to OD of ~0.8 in 1 mL sterile milli-Q water with various concentrations of salts as specified in the figure legends. The germination assays were conducted without heat shock treatments commonly used in germination assay. L-alanine was added to the final concentration of 5mM and OD_{600} was monitored using a spectrophotometer (JENWAY 7305) every 10 min for 120 min. The germination efficiencies (%) in various salt conditions were calculated as the percentage drops in OD_{600} as; $100 \times (1 - \frac{OD_{600}(t)}{OD_{600}(t_0)})$. To examine the impacts of salt to germination efficiency, the data of the last time point (t_{120}) was plotted as a function of salt concentrations.

Effects of ThT to sporulation in liquid RM

Liquid sporulating cultures in RM were prepared in the same manner described above in the section for the spore preparation. After 3.5 hours of incubation in RM, the cultures were supplemented with the final concentrations of 0 µM, 1 µM, 10 µM or 50 µM ThT and incubated at 37°C overnight in a shaking incubator (200 rpm). The cultures were then examined under microscope using LMP-agarose pads. Binary images were made for phase-bright spores and the number of phase-bright spores was determined by the particle analyzer function in imageJ (https://imagej.net/Particle_Analysis).

Wet-heat resistance assay

The spores were prepared as described above in the spore preparation section. Spore suspensions at OD600 ~1.0 were prepared and incubated at 80°C for 30 minutes (heat treatment). The samples were serially diluted and plated onto LB plates (1.5% agar) with three replica plates for each condition and serial dilution. After an overnight incubation in a 37 °C incubator, colonies on LB plates were counted, and the average values of three replica plates were used for analysis. The numbers of colonies appeared with heat-treated samples were divided by the number of colonies appeared with non-heat-treated samples to calculate the survival rate. We also performed time-lapse microscopy assay with the endospores on LB agar pads and quantified the number of endospores that outgrew in 2 hours at 37°C. Data was obtained from three biological replicates with spores prepared each time on different days.

Mathematical model

We model the dynamics of the cytoplasmic and forespore-bound cations with the following coupled differential equations:

$$\frac{dC_c}{dt} = k_2 E - k_{-2}(C_c - E) - k_1 C_c + k_{-1} C_f$$

$$\frac{dC_f}{dt} = k_1 C_c - k_{-1} C_f$$

where C_c is the concentration of cytoplasmic cations, C_f is the concentration of cations bound to forespore and E is the extracellular concentration. We define the following reactions rates:

k_1 : association constant of the cytoplasmic cations to the forespore
k_{-1} : unbinding constant of the cytoplasmic cations to the forespore
k_2 : import rate of the cation pump
k_{-2} : diffusion rate of the cation channel

Considering the development of forespore and increase with time in its negative charge, we assume that k_1 grows monotonically with time. We assume this time dependence as:

$$k_1(t) = \frac{k_{1max} t}{t_m + t}$$

This equation implies that k_1 grows and eventually saturates to a value k_{1max}, and t_m represents the time at which the crossover from linear to zero-order behavior occurs.

Given the lack of quantitative *in vivo* measurements in the literature, we chose to build a phenomenological model in which the values of the parameters are to be interpreted relative to each other, rather than in absolute quantitative terms. Our specific choice of parameter values was made to account for our experimental observations, including forespore-bound potassium and cytoplasmic potassium dynamics during sporulation. For the sake of simplicity, we neglected the potential effect of valinomycin on the active transport term parameterized by k_{-2} and ignored the potential saturation in this term as well, which does not s qualitatively change the results. The parameters used in numerical simulations are $t_m = 1$, $k_2 = 25$, $E = 5$, $k_{-1} = 0.1$, and the simulations were performed using Python.

Image analysis

The time-lapse microscopy images were analyzed with Fiji/ImageJ (National Institutes of Health) (Schindelin et al., 2012). The fore-/endo- spore regions of sporulating cells on each frame of time-lapse microscopy images were manually registered using the ROI (region of interest) manager function in ImageJ. The centroid coordinates, frame and mean pixel intensity values were measured for each ROI using the measure function in ImageJ. Obtained data sets were linked for individual cells based on the coordinate using Trackpy (github.com/soft-matter/trackpy), a Python package for particle tracking. The fluorescence intensities for individual cells were plotted. For the quantification of ThT fluorescence on endospores, a bespoke imageJ macro was developed to threshold the regions of spores based on the brightness in phase-contrast channel. ROIs were registered from the binary images and mean pixel intensities in fluorescence channel were measured for analysis. For the quantification of premature germination, phase-bright and phase-dark spores were counted at frame 30 (10 hours into time-lapse microscopy experiment).

For the estimated probability of premature germination, the confidence intervals were calculated by counting the number of events observed. The calculation was made by using the stats package in scipy (SciPy.org). Numpy (NumPy.org) and Pandas (Pandas.PyData.org) were used to calculate the standard statistical values (mean, standard deviations). All plots were created using the Python packages, matplotlib (github.com/matplotlib) and seaborn (github.com/mwaskom/seaborn).

SI Text: The use of cationic dyes to probe electrical polarity

The use of membrane-permeable fluorescent cationic molecules is a technique for probing membrane potentials of cells. The theory behind this method comes from the Nernst equation, which relates the membrane potential of a cell with the inner and outer concentrations of ions at thermodynamic equilibrium (no net flux of ions):

$$V_m = \frac{RT}{zF} \ln \frac{c_e}{c_i},$$

where R is the universal gas constant, T is the absolute temperature, z is the ionic charge, F is the Faraday constant, c_e and c_i are the external and internal concentrations of the ion respectively. If the ion in question is fluorescent and cationic, and has no specific binding to nucleic acids and other internal molecular structures in cells, then it can be used as a Nernstian dye, where the ratio of external and internal fluorescence follows the Nernst equation with the cell's membrane potential (Ehrenberg et al., 1988). For this study we used two such membrane-permeable cationic fluorescence dyes (ThT and TMRM), but not as probes for membrane potential. This is because the Coulomb interactions between the forespore coat and the cations in the mother-cell cytosol are significant, as can be seen by the spatial distribution of fluorescence dyes within a cell (Figure S2).

Under physiological conditions it is usually assumed that electric fields from surfaces are screened. This model comes from the Poisson-Boltzmann equations (generally referred to as the Guoy-Chapman model), where the electric potential ϕ decays exponentially at a Debye length λ_D,

$$\phi(x) = \phi_0 \exp\left(-\frac{x}{\lambda_D}\right)$$

$$\lambda_D = \sqrt{\frac{\epsilon k_B T}{2 z^2 e^2 c_0}},$$

where ϕ_0 is the potential at the surface, x is the distance from the surface, ϵ is the electric permittivity in the solution, k_B is the Boltzmann constant, T is the temperature, z is the valency of the ions, e is the fundamental charge, and c_0 is the bulk concentration of ions (Bazant et al., 2004). The Guoy-Chapman model for double layers assumes the system is in a steady state, meaning that the concentration profiles of the ions are static in time. By using physiological values, the Debye length in intracellular condition is ~ 1 nm, meaning that the electric field is screened at distances beyond a few nanometres (McLaughlin, 1989). The time scale for diffuse-charge dynamics is given by,

$$\tau_c = \frac{\lambda_D L}{D}$$

where L is the length scale of the system, and D is the diffusion coefficient for the ions (Bazant et al., 2004). By considering the size of the mother cell as a length scale (~ 1 μm) and using a diffusion coefficient typical to aqueous systems (~ 10^{-5} cm^2/sec), this results in a relaxation time to a steady state of 1 μs.

We suggest that the model of charge screening is inappropriate for forespore formation since this system is highly dynamic due to the uptake by ion channels found on the outer membrane of the forespore. Ion channels typically have rate constants of ≥ 10^6 ions/sec (Cahalan et al., 2001), hence the time scale for the ion concentration being reduced locally to the channel is at most 1 μs. This implies that the steady-state Guoy-Chapman model is inappropriate since the time scales are of similar magnitude and a model accounting for the dynamics of the ion channels would need to be developed. In order to accurately describe the electro-diffusion dynamics in sporulation, an alternative mathematical model could be developed, possibly based on the Nernst-Planck-Poisson euqations (Sokalski et al., 2003). Qualitatively, we expect the screening effect to be reduced, resulting in electrostatic forces being significant at distances further than the Debye length. This idea of extended screening length in cytoplasm is supported by experiments carried out in rat astrocytes, where electric fields were measured at micron scale distances from mitochondria in the cytosol (Tyner et al., 2007).

We observed a sudden drop of ThT or TMRM signal upon mother-cell lysis: when the external environment for the spore surface changes from mother-cell cytoplasm to external media. This can be qualitatively explained by the lower concentration of ThT/TMRM externally than inside mother cells. It is also possible that the thickness of the electric double layer becomes thinner due to less ion flux across outer membrane after mother-cell lysis.

Table S1. Resources, related to all figures.

***B. subtilis* strains**		
Strain	**Genotype**	**Source**
PY79	Wildtype	Lab collection
PY79 *ΔgerA*	*gerA*::*spec*^{R}	This study
PY79 *ΔspoIVCA*	*spoIVCA*	(Sandman et al., 1987)
PY79 *ΔgerE*	*gerE36*	(Zheng and Losick, 1990)
PY79 *ΔcotE*	*cotE*::*cm*^{R}	(Zheng et al., 1988)
PY79 *ΔcotB*	*cotB*::*spc*^{R}*(insertion)*	DB068 (Isticato et al., 2001)
PY79 *ΔcotG*	cotGH::*neoR; amyE*::*cotGstopcotH*	(Saggese et al., 2014)
PY79 *ΔcotBG*	*ΔcotGΔcotH*::*neo*^{R}*; amyE*::*cotGstopcotH*	Gift from Loredana Baccigalupi, University of Naples Federico II
PY79 *ΔcotC*	*cotC*::*spec*^{R} *(insertion)*	(Isticato et al., 2004)
PY79 *ΔcotU*	*cotU*::*neo*^{R} *(insertion)*	(Isticato et al., 2004)
PY79 pHluorin	*amyE*::P$_{hyperspank}$-pHluorin, *spec*^{R}	(Martinez et al., 2012)
***E. coli* strains**		
Strain	**Genotype**	**Source**
Top10	Wild type	Lab collection
Top10 pDL30	Carrying the plasmid pDL30	(Garsin et al., 1998; Kuchina et al., 2011)
Top10 ECE174	Carrying the plasmid ECE174	(Kuchina et al., 2011; Middleton and Hofmeister, 2004)
Top10 pTS39	Carrying the plasmid pTS39	This study

Primers		
Name	**Primer description**	**Primer sequence**
AP2	vector_GS351	GTCGCTACCATTACCAGTTGGTCTGG
AP3	amyE_3_GS54	AATGCAGTGGCTGAATCTTCTCC
AP22	ECE174_backbone_rev	TCCTTACGCGAAATACGGGCAG
AP149	cotZterm_pDL30_R	GCCTGCAGGCCTGCAAGCTTTTCCAGCTTGTGTAAACCTATTCATTGTTTTAAAAATATCTC
AP232	pDL30backbone_rev	AAAGGGCCTCGTGATACGC
AP233	gerAA_fwd	aaataggcgtatcacgaggcccttTTGGAACAAACAGAGTTTAAGGAATATATACAC
AP234	gerAA_rev	ttcgcgtaaggaaTCCGGGGATTGCATCAGG
AP235	spec_fwd	tgcaatccccggaTTCCTTACGCGAAATACG

AP236	spec_rev	aaagcagaatgagTGATCCCCCTATGCAAGG
AP237	gerAC_fwd	cataggggatcaCTCATTCTGCTTTCCAAAAG
AP238	gerAC_rev	ggtttgctccggcgcaaatgcagacATTTGTTTGCGCCTTTCG
AP239	pDL30_backbone_fwd	GTCTGCATTTGCGCCGGA
AP240	ECE174_backbone_rev	CATGTGCTGTCCTGCATTAATG
AP247	ECE174_backbone_fwd	CAGTACAATCTGCTCTGATGCC
AP252	gerA_5_int_check	CCATTTATGTATCCCTCCATAACGGT
AP253	gerA_3_int_check	GCCTGATCGCAGAAGGAAAGAC

Supplemental references

Bazant, M.Z., Thornton, K., Ajdari, A., 2004. Diffuse-charge dynamics in electrochemical systems. Phys. Rev. E - Stat. Physics, Plasmas, Fluids, Relat. Interdiscip. Top. 70, 24. https://doi.org/10.1103/PhysRevE.70.021506

Cahalan, M.D., Wulff, H., Chandy, K.G., 2001. Molecular properties and physiological roles of ion channels in the immune system. J. Clin. Immunol. 21, 235–252. https://doi.org/10.1023/A:1010958907271

Depauw, A., Dossi, E., Kumar, N., Fiorini-Debuisschert, C., Huberfeld, G., Ha-Thi, M.-H., Rouach, N., Leray, I., 2016. A Highly Selective Potassium Sensor for the Detection of Potassium in Living Tissues. Chemistry 22, 14902–14911. https://doi.org/10.1002/chem.201602209

Ehrenberg, B., Montana, V., Wei, M.D., Wuskell, J.P., Loew, L.M., 1988. Membrane potential can be determined in individual cells from the nernstian distribution of cationic dyes. Biophys. J. 53, 785–794. https://doi.org/10.1016/S0006-3495(88)83158-8

Garsin, D.A., Paskowitz, D.M., Duncan, L., Losick, R., 1998. Evidence for common sites of contact between the antisigma factor SpoIIAB and its partners SpoIIAA and the developmental transcription factor σ(F) in *Bacillus subtilis*. J. Mol. Biol. 284, 557–568. https://doi.org/10.1006/jmbi.1998.2201

Isticato, R., Cangiano, G., Tran, H.T., Ciabattini, A., Medaglini, D., Oggioni, M.R., De Felice, M., Pozzi, G., Ricca, E., 2001. Surface display of recombinant proteins on Bacillus subtilis spores. J. Bacteriol. 183, 6294–301. https://doi.org/10.1128/JB.183.21.6294

Isticato, R., Esposito, G., Zilhão, R., Nolasco, S., Cangiano, G., De Felice, M., Henriques, A.O., Ricca, E., 2004. Assembly of Multiple CotC Forms into the *Bacillus subtilis* Spore Coat. J. Bacteriol. 186, 1129–1135. https://doi.org/10.1128/JB.186.4.1129-1135.2004

Jarmer, H., Berka, R., Knudsen, S., Saxild, H.H., 2002. Transcriptome analysis documents induced competence of *Bacillus subtilis* during nitrogen limiting conditions. FEMS Microbiol. Lett. 206, 197–200.

Kralj, J.M., Hochbaum, D.R., Douglass, A.D., Cohen, A.E., 2011. Electrical spiking in *Escherichia coli* probed with a fluorescent voltage-indicating protein. Science 333, 345–8. https://doi.org/10.1126/science.1204763

Kuchina, A., Espinar, L., Çağatay, T., Balbin, A.O., Zhang, F., Alvarado, A., Garcia-Ojalvo, J., Süel, G.M., 2011. Temporal competition between differentiation programs determines cell fate choice. Mol. Syst. Biol. 7, 1–11. https://doi.org/10.1038/msb.2011.88

Martinez, K.A., Kitko, R.D., Mershon, J.P., Adcox, H.E., Malek, K.A., Berkmen, M.B., Slonczewski, J.L., 2012. Cytoplasmic pH response to acid stress in individual cells of *Escherichia coli* and *Bacillus subtilis* observed by fluorescence ratio imaging microscopy. Appl. Environ. Microbiol. 78, 3706–14. https://doi.org/10.1128/AEM.00354-12

McLaughlin, S., 1989. The Electrostatic Properties of Membranes. Annu. Rev. Biophys. Biophys. Chem. 18, 113–136. https://doi.org/10.1146/annurev.bb.18.060189.000553

Middleton, R., Hofmeister, A., 2004. New shuttle vectors for ectopic insertion of genes into *Bacillus subtilis*. Plasmid 51, 238–45. https://doi.org/10.1016/j.plasmid.2004.01.006

Prindle, A., Liu, J., Asally, M., Ly, S., Garcia-Ojalvo, J., Süel, G.M.G.M., 2015. Ion channels enable electrical communication in bacterial communities. Nature 527, 59–63. https://doi.org/10.1038/nature15709

Roder, P., Hille, C., 2014. ANG-2 for quantitative Na+ determination in living cells by time-resolved fluorescence microscopy. Photochem. Photobiol. Sci. 13, 1699–710. https://doi.org/10.1039/c4pp00061g

Saggese, A., Scamardella, V., Sirec, T., Cangiano, G., Isticato, R., Pane, F., Amoresano, A., Ricca, E., Baccigalupi, L., 2014. Antagonistic role of CotG and CotH on spore

germination and coat formation in Bacillus subtilis. PLoS One 9, 1–8. https://doi.org/10.1371/journal.pone.0104900

Sandman, K., Losick, R., Youngman, P., 1987. Genetic analysis of Bacillus subtilis spo mutations generated by Tn917-mediated insertional mutagenesis. Genetics 117, 603–617. https://doi.org/10.1128/JB.01343-06

Schindelin, J., Arganda-Carreras, I., Frise, E., Kaynig, V., Longair, M., Pietzsch, T., Preibisch, S., Rueden, C., Saalfeld, S., Schmid, B., Tinevez, J.-Y., White, D.J., Hartenstein, V., Eliceiri, K., Tomancak, P., Cardona, A., 2012. Fiji: an open-source platform for biological-image analysis. Nat. Methods 9, 676–82. https://doi.org/10.1038/nmeth.2019

Sokalski, T., Lingelfelter, P., Lewenstam, A., 2003. Numerical solution of the coupled Nernst-Planck and Poisson equations for liquid junction and ion selective membrane potentials. J. Phys. Chem. B 107, 2443–2452. https://doi.org/10.1021/jp026406a

Sterlini, J.M., Mandelstam, J., 1969. Commitment to sporulation in *Bacillus subtilis* and its relationship to development of actinomycin resistance. Biochem. J. 113, 29–37.

Tyner, K.M., Kopelman, R., Philbert, M.A., 2007. “Nanosized voltmeter” enables cellular-wide electric field mapping. Biophys. J. 93, 1163–1174. https://doi.org/10.1529/biophysj.106.092452

Zheng, L., Losick, R., 1990. Cascade regulation of spore coat gene expression in Bacillus subtilis. J. Mol. Biol. 212, 645–660. https://doi.org/10.1016/0022-2836(90)90227-D

Zheng, L.B., Donovan, W.P., Fitz-James, P.C., Losick, R., 1988. Gene encoding a morphogenic protein required in the assembly of the outer coat of the *Bacillus subtilis* endospore. Genes Dev. 2, 1047–54. https://doi.org/10.1101/gad.2.8.1047